



Advances in top–down and bottom–up surface nanofabrication: Techniques, applications & future prospects

Abhijit Biswas ^{a,*}, Ilker S. Bayer ^b, Alexandru S. Biris ^c, Tao Wang ^a, Enkeleda Dervishi ^c, Franz Faupel ^d

^a Center for Nano Science and Technology (NDnano), Department of Electrical Engineering, University of Notre Dame, IN 46556, USA

^b Center for Biomolecular Nanotechnologies, Smart Materials Platform, Italian Institute of Technology, Lecce 73010, Italy

^c Nanotechnology Center, University of Arkansas at Little Rock, Little Rock, AR 72204, USA

^d Chair For Multicomponent Materials, Institute for Materials Science, Christian Albrechts University of Kiel, D-24143, Kiel, Germany

ARTICLE INFO

Available online 16 November 2011

Keywords:

Nanofabrication
Lithography
Self assembly
Vapor phase deposition
Nanocomposites

ABSTRACT

This review highlights the most significant advances of the nanofabrication techniques reported over the past decade with a particular focus on the approaches tailored towards the fabrication of functional nano-devices. The review is divided into two sections: top–down and bottom–up nanofabrication. Under the classification of top–down, special attention is given to technical reports that demonstrate multi-directional patterning capabilities less than or equal to 100 nm. These include recent advances in lithographic techniques, such as optical, electron beam, soft, nanoimprint, scanning probe, and block copolymer lithography. Bottom–up nanofabrication techniques—such as, atomic layer deposition, sol–gel nanofabrication, molecular self-assembly, vapor-phase deposition and DNA-scaffolding for nanoelectronics—are also discussed. Specifically, we describe advances in the fabrication of functional nanocomposites and graphene using chemical and physical vapor deposition. Our aim is to provide a comprehensive platform for prominent nanofabrication tools and techniques in order to facilitate the development of new or hybrid nanofabrication techniques leading to novel and efficient functional nanostructured devices.

© 2011 Elsevier B.V. All rights reserved.

Contents

1. Introduction	3
2. Top–down nanofabrication methods	3
2.1. Optical lithography	3
2.2. E-beam lithography	4
2.3. Soft lithography	5
2.4. Nanoimprint lithography	5
2.5. Block copolymer lithography	7
2.6. Scanning probe lithography	9
3. Bottom–up nanofabrication methods	9
3.1. Atomic layer deposition	10
3.2. Sol–gel nanofabrication	11
3.3. Molecular self assembly	14
3.4. Vapor phase deposition of nanomaterials	16
3.5. DNA-scaffolding for nanoelectronics	19
4. Conclusion and perspective on future advances in nanofabrication and technological implications	22
Acknowledgements	24
References	24

* Corresponding author. Tel.: +1 574 631 5619; fax: +1 574 631 4393.
E-mail address: abiswas@nd.edu (A. Biswas).

1. Introduction

Nanofabrication involves processes and methods of constructing engineered nanostructures and devices having minimum dimensions lower than 100 nm. This technology is the basis for nearly every aspect of nanomaterials research and development with a focus on their use for complex multifunctional devices with applications spanning over a wide technological field from energy harvesting and storage, electronics, sensing, medicine and human health care etc. The last decade has witnessed the development of a variety of nanofabrication techniques fulfilling high expectations surrounding nanotechnology and nanofabrication [1–10]. This has facilitated unprecedented growth of knowledge and thorough understanding of the characteristics specific to many fascinating nanostructures, their properties related to a particular application, and the integration of engineered nanomaterials into multifunctional devices.

Large-scale, commercial implementation of nanofabrication techniques provide exciting opportunities for the unprecedented development of information technologies and advanced micro and nanoelectronic devices such as developing super-high-density microprocessors and memory chips. Advances in nanofabrication techniques are expected to lead to technological breakthroughs including storing each data bit in a single atom that might even be able to represent a sequence of 8 bits processed as a single unit of information (known as a byte). It is believed that future developments in novel nanofabrication-based technologies will lead to advanced technology applications in areas such as nano-medicine with a focus on individualized health care, advanced functional materials with tunable properties, sensors, surfaces with controlled properties and optics [1,2,6,11].

But in order for all these applications to become reality, the major need is for the development of engineering nanofabrication approaches that would allow almost with atomic precision the development or the processing of materials with the desired structural, mechanical, optical, magnetic or electronic properties. Given the large breadth of such applications, generally, the nanofabrication methods are divided into two major categories: “top–down” and “bottom–up” methods according to the processes involved in creating nanoscale structures. A top–down approach corresponds to using nanofabrication tools that are controlled by external experimental parameters to create nanoscaled structures/functional devices with the desired shapes and characteristics starting from larger dimensions and reducing them to the required values [2,6]. On the other hand, bottom–up approaches seek to have molecular or atomic components built up into more complex nanoscale assemblies or directed self-assemblies based on complex mechanisms and technologies [1]. Basically, this area of nanofabrication uses atoms or small molecules as the building blocks of multi-level structures that perform various operations and is extremely promising since it could lead to no waste or unused materials. In this review, we describe prominent top–down and bottom–up techniques for the fabrication of nanostructures and devices that have been developed and reported in the literature since 2000. This review compliments to the available review articles on nanofabrication techniques. New nanofabrication tools or combination of standard nanofabrication approaches may be needed in the future research and development of new nanomaterials including multicomponent nanomaterials. The aim of this review is to provide a comprehensive platform on prominent top–down and bottom–up nanofabrication techniques that may be useful to the researchers seeking development of new or hybrid nanofabrication techniques, particularly for the controlled fabrication of complex and multicomponent nanomaterials that are needed for advanced functional applications. In addition to other techniques, we have attempted to cover physical and chemical vapor phase deposition, and sol–gel method that can be used for the fabrication of complex and multicomponent nanomaterials and nanostructures. Our discussions include nanofabrication techniques that are used for fabrication of nanomaterials and structures ≤ 100 nm either or both in horizontal and vertical

dimensions. Finally, we present a perspective on future directions of nanofabrication and the technological implications of further advances in nanofabrication techniques.

2. Top–down nanofabrication methods

Various methods of lithography are used in the top–down approach, including serial and parallel techniques for patterning two-dimensional nanoscale features [2,6]. In conventional lithography, required material is usually protected by a mask and the exposed material is etched away. Chemical etching using acids or mechanical etching using ultraviolet light, X-rays, or electron beams is performed that determines the feature resolutions of the final product. Other top–down approaches include methods such as scanning probe lithography, nanoimprint lithography and block co-polymer lithography, etc.

2.1. Optical lithography

The microelectronics industry frequently uses optical lithography for patterning nanoscale features. Optical lithography techniques were first introduced in the 1960's to fabricate integrated circuits [2,6,12]. Conventional optical or photolithographic approaches use light that is collimated through a quartz plate supporting a chromium coating to create patterns on a surface [2]. The quartz plate which serves as a mask is placed in contact or close proximity to the resist-coated wafer [2]. The photoresist is an organic, light-sensitive material that can be coated on semiconductor wafers. There are two possible transformations that a photoresist polymer can undergo upon exposure to light. If a *positive* photoresist material is illuminated, the exposed regions will present a higher solubility in the developing solutions. The photoresist that was exposed can then be removed from the solution. A *negative* photoresist material becomes cross-linked when exposed to light—and will be characterized by a high solubility in the developing solution. After the interaction with the developing solution, the areas that were not exposed to light will be etched away. The remaining photoresist patterns will therefore protect the substrate from being removed and/or from the deposition of additional materials. The photoresist can be removed after the desired process is completed leaving behind the pattern design on the substrate [2].

Conventional photolithography is a simple technique that makes possible a resolution of about 1 μm using light of 400 nm [2,13]. To achieve a better resolution, more advanced photolithography techniques involve placing a mask at the focal plane and projecting onto a photoresist coating [2]. In projection lithography, a lens is inserted between the mask and the wafer in order to image the mask onto the surface of the resist [2].

The most important parameter in optical projection lithography is the lens' numerical aperture. The numerical aperture is defined as follows: $NA = n \sin(i)$ where n is the refraction index of the medium through which light travels and i is the maximum angle of light collected at the focal point [2,6]. Using the Rayleigh criterion, the minimum distance that can be imaged by the lens in ideal lens and light conditions is given by [2,6,13,14].

$$L_{\min} = 0.61 \cdot \lambda / NA$$

With the introduction of the k factor for real conditions, the formula becomes:

$$L_{\min} = k \cdot \lambda / NA$$

With a k factor of around 0.3, $\lambda = 157$ nm and $NA = 0.6$, $L_{\min} < 80$ nm is currently in production [6,13].

A large number of variations in the basic projection lithography process exist. For example, the reticle can be modified in complex

ways to allow the phase of the light to vary as it passes through leading to constructive and destructive interference at the focal plane, allowing tighter lines and spaces, a process known as “phase shift lithography” [15]. The reticle can also be designed with complex shapes that are a distorted version of the desired pattern, but interferences of the light with the mask, optical column, and wafer result in the actual desired pattern, a process known as “optical proximity effect correction” [16]. Further, the light incident on the reticle can be tilted off of the normal so that higher diffraction orders make it through the column, which results in higher spatial resolution, a process called “off-axis illumination” [17].

Other improvements include “immersion lithography”, in which the space between the lens and the wafer is filled with water. Due to the higher index of refraction, a higher numerical aperture, and therefore a smaller feature pitch, is achieved [18]. Another recent improvement is called “double pattern” lithography in which a subset of the final pattern is exposed and processed, followed by the exposure of the remaining patterns in a subsequent process in order to complete the pattern. This eliminates interference of very closely spaced patterns on either exposure while taking advantage of the ability to make very fine alignments [19]. Most recently, it has been shown that the benefits of double patterning can be extended to <32 nm logic using selective double pass patterning [20].

Naturally, the ultimate patterning density can be increased with decreasing illumination wavelength. In order to circumvent wavelength limitations, current efforts are directed toward developing “extreme ultraviolet lithography” or “EUV” (which actually uses long wavelength X-rays), where transmitted light reticles are replaced by reflected light masks, and Bragg scattering from multiple, nm-thick layers creates the desired pattern [21]. EUV is under development by the semiconductor industry in the hopes of extending patterning resolution well beyond the current 32 nm node, but many problems are yet to be overcome [22].

A new approach to photolithography called Resolution Augmentation through Photo-Induced Deactivation ‘RAPID’ was recently demonstrated. Multi-photon absorption from a pulsed laser of 800 nm excitation induces the cross-linking process within the structure of a polymeric photoresist material. One photon absorption process of an 800 nm light excitation simultaneously deactivates the photopolymerization (Fig. 1). The phase-shaping of the deactivation beam therefore makes it possible to construct nanoscale features with scalable resolution, of as low as 40 nm [3]. Various two dimensional and three dimensional morphologies with dimensions of a fraction of the wavelength of the optical excitation employed may be created by this method for applications in electronics, optics, and biomedical devices [3,4].

2.2. E-beam lithography

Electron beam (e-beam) lithography is a commonly used top-down fabrication method to create various nanostructures and devices [23]. E-beam lithography was originally developed for manufacturing integrated circuits. The approach of e-beam lithography includes creation of low-dimensional structures in the resist that are subsequently transferred to the substrate material by etching. E-beam lithography is considered superior over conventional photolithography. The advantage of e-beam lithography lies in the fact that it overcomes the diffraction limit of light that helps create features in the nanometer range. It is a mask-less form of lithography and very popular in photomask-making for photolithography.

Typical e-beam lithography includes electron beam direct write process, where an electron beam of reduced dimensions is exposed directly to the top surface of a resist-coated material. The technique involves the 2D scanning of an electron beam over the surface of a material that has been previously covered with any type of electron-reactive resist. Therefore, this is a relatively low throughput process. Compared to photolithography, for example, it has rather low productivity because it is a serial process and often partially manual. As a result, the writing speed and transfer rate for the design data are limited [24].

More advanced e-beam lithography includes electron projection lithography. In electron projection lithography, a combination of high precision masks and lens systems is used to expose a large scale pattern onto a substrate coated with resist [26]. It is capable of a huge penetration depth of electrons [25]. A 100 nm thick nitride material is used as a mask in the projection lithography. The electron optical system’s rear focal plane contains an aperture that blocks the highly scattered electrons. The trajectories of the electrons allowed to pass through the membrane are only slightly altered and ultimately create a high-contrast image on the wafer surface or substrate [24,26]. The short wavelength and energy density of the electron beam allows the fabrication of ultra-fine feature sizes. It has been used to successfully fabricate many nanoscale devices [26]; including 10 nm thick read heads used in the magnetic recording applications. E-beam lithography combined with hydrogen silsesquioxane (HSQ)-based resist engineering has resulted in the ability to manufacture and use nanoscaled thin-film heads for advanced magnetic recording at densities of Terabit/square inch and higher [27].

A two-step technique for writing at the nanoscale has been developed by F. Bretagnol et al. [28]. The authors demonstrated the production of patterns that are bio-adhesive in a non-bio-adhesive substrate. The nanofabrication process is based on the combination of plasma-based formation of a polyethylene oxide film that is used for protein-repelling and the subsequent construction of nanoscale

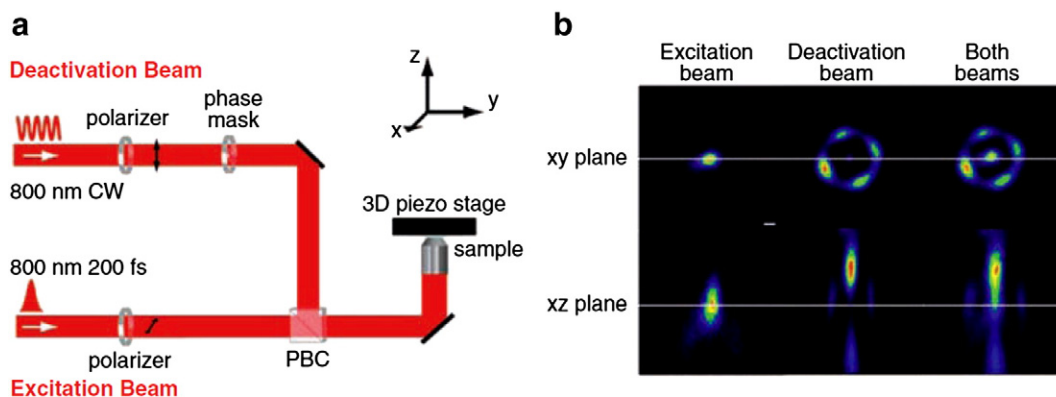


Fig. 1. [a] A schematic illustration of the experimental setup for RAPID lithography. A pulsed excitation beam and a phase-shaped, continuous wave (CW) deactivation beam (PBC: Polarizing Beam Cube) are used in RAPID lithography [b] Luminescence images of the cubes of the excitation beam, the deactivation beam, and both beams together. The scale bar in the upper left image is 200 nm. The approximate centers of the focal regions are indicated by the long white lines. Fig. reproduced from Ref. [3] with kind permission, © The American Association for the Advancement of Science.

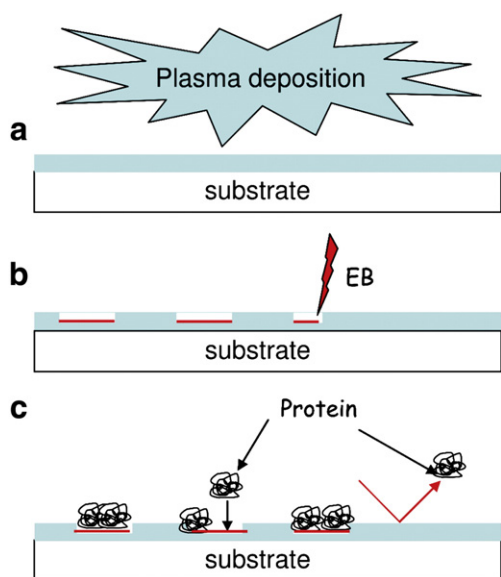


Fig. 2. Schematic illustrations of the nanofabrication steps of bio-adhesive in a non-bio-adhesive substrate using e-beam lithography (a) The deposition of non-bio-adhesive matrix (PEO-like layer ~10 nm) onto the substrate by plasma polymerization of diethylene glycol dimethyl ether. (b) Exposure of the PEO-like layer to the electron beam (EB) results in the chemical modification and removal of the material. (c) Biomolecules get confined inside the arrays as a result of incubation of the patterned surface in protein solution. Fig. reproduced from Ref. [28] with kind permission, © Institute of Physics Publishing Ltd.

large bio-adhesive patterns by electron beam lithography that alters the concentration of the ether bonds of the coating within the matrix [28]. Fig. 2 illustrates schematically this fabrication and controlled writing process.

Most recently, arrays of vertically oriented gold and copper nanopillars with diameters down to 25 nm based on patterning polymethylmethacrylate were created by e-beam lithography. Fig. 3 shows SEM images of the prepared Au nanopillars by e-beam lithography [29]. Such nanopillars could find excellent applications in field emission applications, sensing, energy harvesting/conversion, or nanomedicine. The key element is to have the ability of controlling their structural morphologies such that it would match certain applications.

2.3. Soft lithography

Soft lithography has been developed as an alternative for photolithography [30–40]. The soft lithography method is used to transfer a thin, molecular pattern onto a surface. The main advantage of soft lithography is that it does not require expensive clean room processing

steps once the reusable mold is developed; this method also makes it possible to transfer wet layers more readily than would be possible using other techniques. This approach usually employs the use of a microscale replica that can be generated by the controlled molding of a specific polymer, such as poly(dimethyl siloxane) (PDMS) [41]. Microstamping, stencil patterning, and microfluidic patterning are the three main soft lithography processes. In microstamping, the molecules (e.g., peptides, proteins, polysaccharides) are positioned onto the stamp surface and subsequently transferred to another surface, thereby producing a self-assembled monolayer (SAM) [41]. The microcontact or microstamp printing is advantageous because it allows the single step formation of large scale patterns. Another advantage is the flexibility of these stamps. They can be used in a desired shape to fit any surface topography.

Microstamp printing has been employed to fabricate magnetic nanostructures to study vortex–single domain transition in Co nanodots (~100 nm) [42]. In another application, a single protein array was deposited with 80-nm resolution by using a PDMS stamp that presented a high Young's modulus [43]. Microfluidic patterning uses a PDMS mold to form microsized channels on the surface of a substrate which can then further be employed to deposit fluid materials [2,41]. Microfluidic patterning was successfully used for the controlled deposition of cells for various applications involving tissue-engineering [41].

An alternative approach to soft lithography without using PDMS has been proposed by Y.S. Kim et al. [44]. The authors employed a mold made from a UV-curable polyurethane acrylate. For the soft-molding, a water-soluble sulfonated polystyrene (SPS) was used. In addition, multilayer deposition was performed to generate an additional adhesion-promotion layer between the polymeric layer and the surface of the substrate [44]. This approach overcomes the limitations of the PDMS-based soft lithography, such as the lateral mold collapse of PDMS that makes it difficult to generate high-density arrayed nanostructures. The soft lithography without using PDMS allows pattern transfer of highly ordered polymeric nanostructures (80 nm width × 400 nm height) on different substrates including glass and flexible films of polymers [44].

2.4. Nanoimprint lithography

Nanoimprint lithography is an important top-down lithographic method for advanced nanostructure fabrication. This nanofabrication method is capable of high-throughput patterning of nanostructures with high resolution. Nanoimprint lithography is usually based on the mechanical embossing principle. The method can be employed to generate patterns with superior resolutions than conventional lithographic techniques that are limited by either beam scattering or light diffraction. Uniform mechanical deformation of the materials that are used as resists generates the replica of the initial pattern. Hence, the

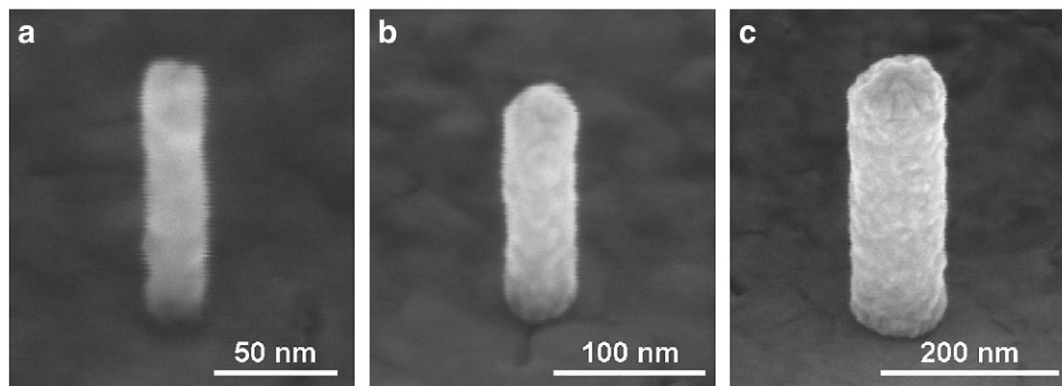


Fig. 3. SEM images of Au nanopillars prepared for compression tests with diameters of 25, 50, and 100 nm prepared by e-beam lithography. Fig. reproduced from Ref. [29] with kind permission, © American Chemical Society.

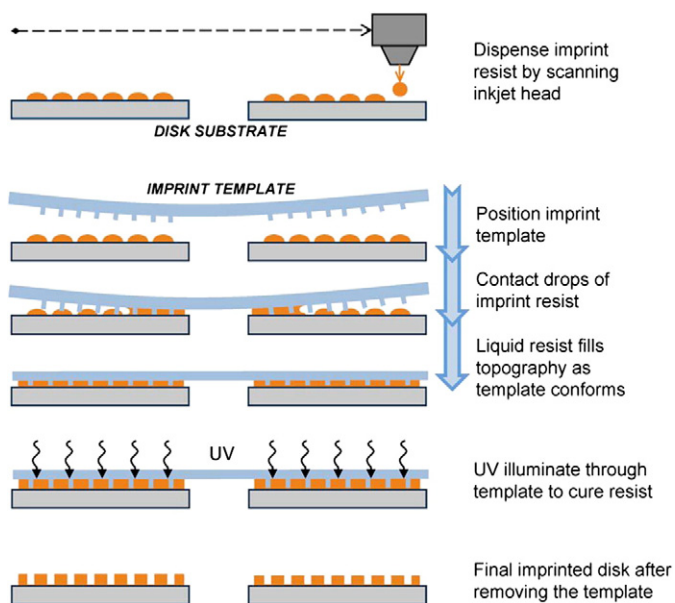


Fig. 4. Process flow for imprint patterning of hard disk substrates. Fig. reproduced from Ref. [4] with kind permission, © American Vacuum Society.

approach allows to overcome limitations related to resolution caused by the diffraction or scattering of the beam. The resist material usually consists of either a heat or UV exposure curable monomer or a polymeric material. The adhesion of the resist with the template can be controlled by choosing the desired properties of the resist [45]. Imprint lithography involves a 3D patterning process in which vertically arranged topographic layers are used to construct the molds. A broad range of materials with various properties can be used.

Nanoimprint lithography methods can be classified into three categories: They are thermoplastic, photo, and electrochemical nanoimprints methods. The method of thermoplastic lithography, the earliest form of nanoimprint lithography, was originally developed by S. Chou's group at Princeton University [46]. The original process involved deposition of a fine film of a thermoplastic polymer (imprint resist) by spin coating onto the surface of the sample. This was followed by pressing together a mold with prefabricated 3D patterns with the sample under a certain pressure. Subsequent heating above the polymer's glass transition point resulted in the formation of the pattern of the mold in the softened polymeric film. A post thermal cooling process involved the removal of original mold from the surface of the sample, while keeping the pattern resist on the substrate [46]. Reactive ion etching is usually performed to carry out the pattern-transfer process to the substrate.

Photo nanoimprint lithography involves coating of the sample surface with a UV-curable liquid resist. This is followed by the process of pressing an optically transparent mold into the substrate and the

subsequent solidification of the resist under UV radiation. Electrochemical nanoimprinting is another approach that uses a stamp fabricated from a superionic conductor (silver sulfide). The process involves an applied voltage that initiates electrochemical etching when the stamp is in contact with the metal surface. Subsequent formation of metal ions get transferred from the film to the stamp [47].

During the last few years, there has been significant growth in literature describing various nanostructure and device fabrication processes using nanoimprint lithography [48–79]. Monolayers of molecular rotaxanes sandwiched between metal electrodes have been used to form molecular-electronic devices at the nanoscale by using nanoimprint lithography [41]. Current–voltage behavior presenting elevated on-off ratios along with reversible switching characteristics has been reported for these devices, which could therefore act as basic components for the next-generation electronic circuits [80].

Recently, a step-and-flash imprint lithography (SFIL) approach has been reported for the patterning of magnetic substrates [4]. The ever-expanding need for memory storage devices with higher storage density and capability is primarily responsible for the shift towards patterned media hard disks. If patterning of the magnetic domain boundaries can be achieved, the practical limitations of the superparamagnetic effect of magnetic grains (thermal switching of magnetization) could be avoided. Patterned-based magnetic hard disks could be intensively used since they could provide data storage of densities exceeding 10^{12} bits/in² (1 Tbit/in²). However, such a shift in the storage technology will require lithography of extremely high resolution and precision, as well as very low cost to make such devices marketable [4].

In SFIL lithography, a photocurable pre-polymer solution is used to replicate the topography of a rigid mold. A hard disk can be patterned using SFIL lithography in the same way it is done in semiconductor device fabrication [4]. Fig. 4 shows the process for the patterning of hard disk surfaces. The imprint patterning process flow involves deposition of a liquid acrylate resist by an ink-jet printing process onto the surface of the substrate. The next step involves lowering the template to the point at which there is contact with the resist. Capillarity will cause the resist to flow and fill the volumes between the substrate and the morphologies of the template which will polymerize under UV irradiation (Fig. 4) [4].

The patterned media process expanded into large scale manufacturing opens the possibility of achieving hard disk storage devices with a storage superior to 1 Tbit/in² [4].

Another application of nanoimprint lithography is in the area of nanofluidics [81–84] that involves the understanding of complex molecular fluid behavior in small sizes, along with molecular detection down to a single molecule [85]. The approach is based on the interaction and transportation of various biological molecules, such as single- or double-stranded DNA, proteins, with nanosized channels (~50 nm). This is a promising approach for the high sensitivity detection and understanding of the possible interactions between various molecules [45,86,87].

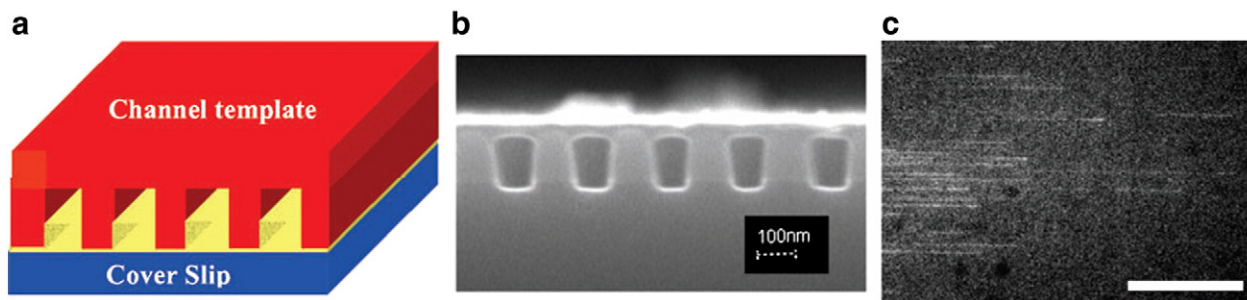


Fig. 5. (a) Schematic illustration of the fabrication of nanofluidic channel that uses a template mold for imprinting. This results in a thin polymer layer leaving unfilled and self-enclosed channels. (b) A typical SEM micrograph of imprinted nanofluidic channels with cross sections of 75 nm × 120 nm. (c) Fluorescent images showing the stretching of 103 kb long T5 phage DNA in the nanochannels reaching about 95% (scale bar 50 μm). Fig. reproduced from Ref. [45] with kind permission, © Institute of Physics Publishing Ltd.

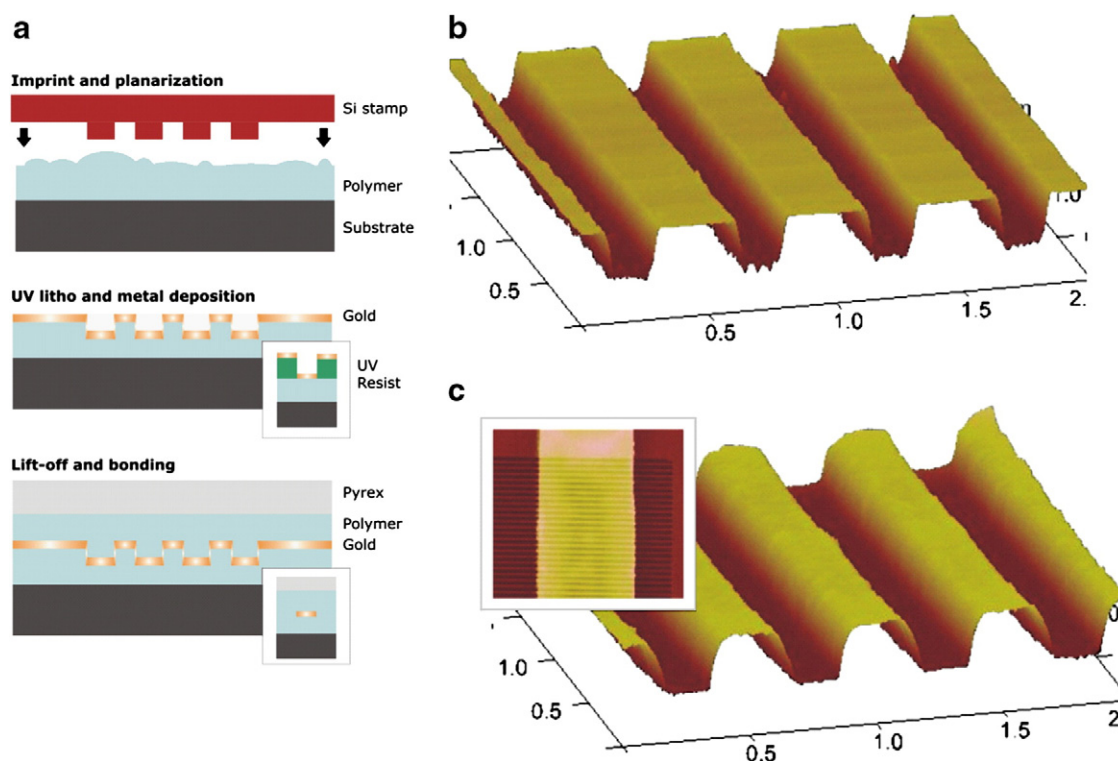


Fig. 6. (a) Schematic illustration of the fabrication process for long-range plasmonic waveguides. A silicon stamp (fabricated via electron-beam lithography and etching) is pressed into the nanoimprinted lithography resist, which is spun on a silicon substrate. This is followed by thermal nanoimprint and separation. Strip waveguides are subsequently created via UV-lithography, gold deposition and lift-off process. Inset figures on the (a) part show the transverse cross-section of the patterned waveguide. Typical atomic force microscope (AFM) images (horizontal axes in micrometer) of (b) silicon stamp with the grating with a ridge height ~ 27 nm and (c) shows an imprinted grating with period 514 nm and protrusion depth 28 nm. The inset figure on the (c) part shows a top view of an AFM image of the $8 \mu\text{m}$ -wide metal stripe deposited on the nanoimprint molded polymer surface. Fig. reproduced from Ref. [91] with kind permission, © Institute of Physics Publishing Ltd.

A simple method to fabricate nanofluidic channels of controllable channel diameter and height was developed by using a modified imprinting technique [88,89]. The process involves the use of a thin film of a polymer during the imprinting process. An enclosed nanoscale channel structures is formed by the polymer that does not entirely cover the asperities of the mold (Fig. 5(a)) [45]. L. J. Guo et al. have demonstrated a biological application by introducing DNA strands in such nanotubular structures [45]. An over 90% stretch was reported to take place in the nanosized channels having a section size of $\sim 120 \text{ nm} \times 75 \text{ nm}$ (Fig. 5(b) and (c)). This work demonstrated that the nanodimensional channels are excellent systems to study both

the static and the dynamic behavior of DNA molecules in confined spaces. The applications that were mentioned included the possible extremely fast (minutes) mapping of various genomic DNA segments [86,88,79,89].

In addition, the fabrication by nano-imprint mold fabrication of extremely long (over 1.5 cm) fluidic channels of uniform diameters (11–50 nm) could be promising for highly sensitive biochemical sensors [90].

Nanoimprint lithography has been used for the fabrication of nanoscale optical devices and components. Plasmonic component fabrication for advanced optical devices has been achieved by nanoimprint lithography [91]. Plasmonic nanomaterials with different surface plasmon modes (i.e., propagating or localized) are promising candidates for nanophotonic components [91]. Nanoimprint in combination with photolithography has been employed to fabricate long-range plasmonic waveguides for ultracompact nanophotonic components (Fig. 6) [92].

The combination of nanoimprint and photolithography processes includes the pressing of a silicon stamp made by electron beam lithography into the nanoimprint lithography resist spun on a silicon substrate. This leads to the fabrication of plasmonic strip waveguides using a standard UV-lithography process, gold deposition, and lift-off (Fig. 6) [92].

2.5. Block copolymer lithography

Block copolymer lithography involves a combination of bottom-up self-assembly and top-down lithographic processes. The self-assembly of block copolymers is represented by two polymeric chains linked together. The self-assembly of thin films of block copolymers can result in domains with high periodicity (10 nm within a template or highly elaborate patterns [93–110]. Topographically or chemically patterned templates are used to control the orientation and

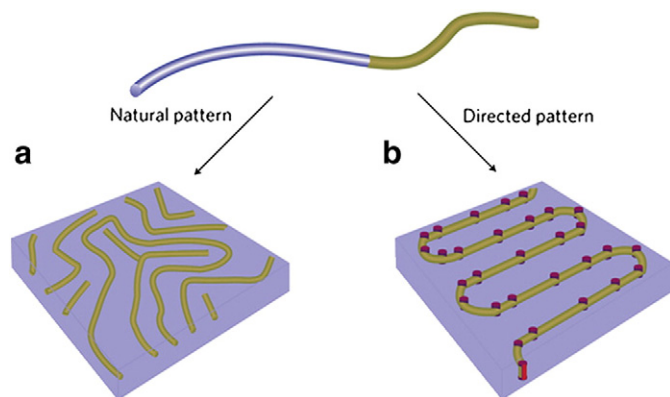


Fig. 7. (a) Schematic illustration of the natural self-assembly of diblock-copolymer thin films that results in un-defined patterns (light purple color corresponds to the majority block-copolymer phase and brown color corresponds to the minority block-copolymer phase). (b) Sparse template represents an array of posts prepared by electron-beam patterning of an inorganic resist (dark purple color) that generates highly organized and asymmetric patterns. Fig. reproduced from Ref. [93] with kind permission, © Nature Publishing Group.

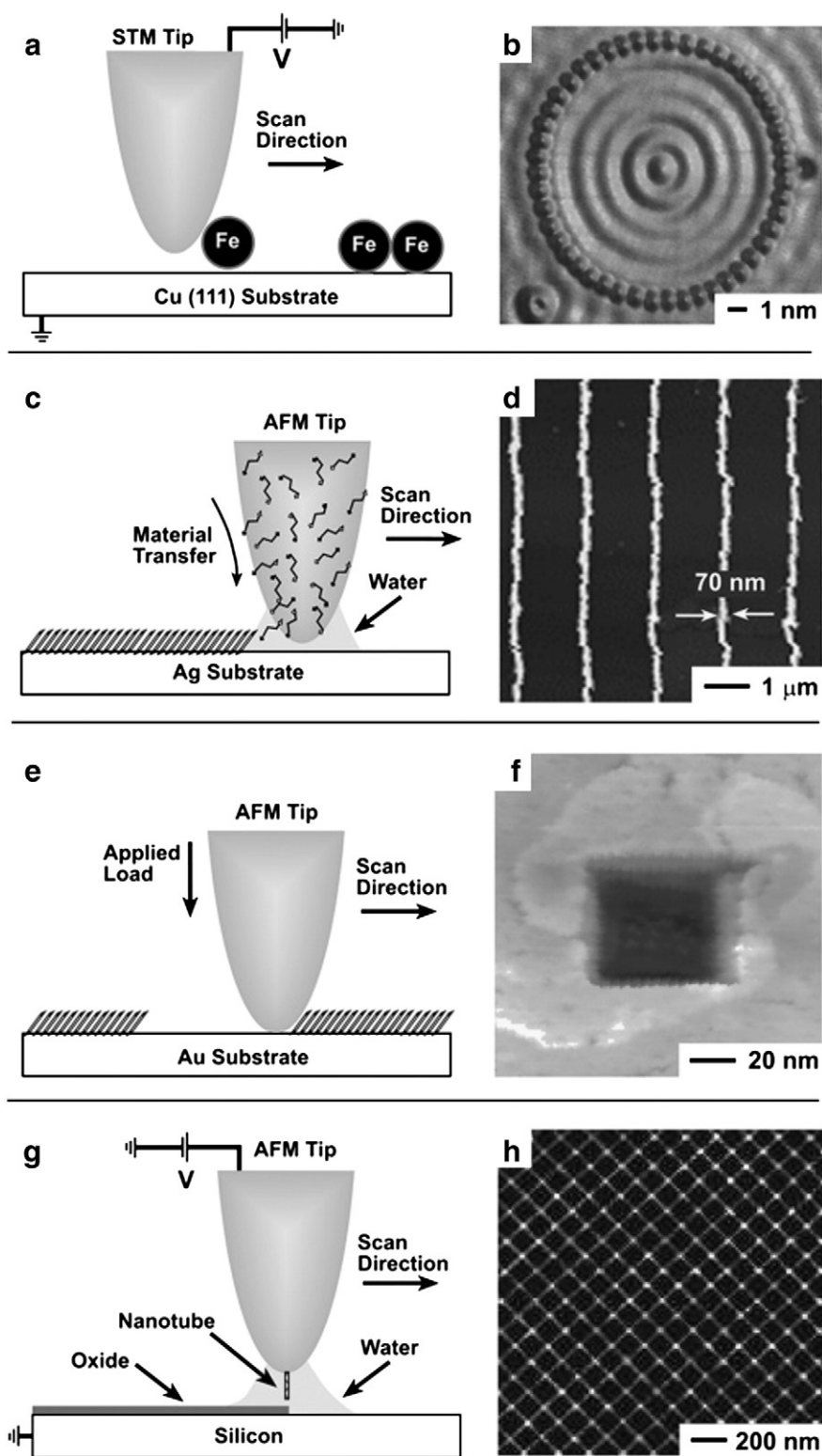


Fig. 8. Schematic representations of approaches to SPL and the nanometer-scale features produced. Fig. reproduced from Ref. [2] with kind permission, © American Chemical Society.

placement of block-copolymer domains. Recent research has shown that, by accurately controlling properties such as the functionality or the molecular weight of the block copolymers, pattern generation can be achieved via molecular engineering. According to J. Poelma and C. Hawker [93], using a combination of molecular interactions and topology, advanced surface chemistry processes, and structural control, it may be possible to fabricate and to design defect-free

structures formed of sub-10-nm morphologies with various dimensions and geometries [111–114]. For example, an organization of nanoscaled structures was created by electron-beam patterning using the molecular weight of an inorganic resist to control the block copolymer domain sizes [115]. The ability to create 20 nm structures which could be rotated by 90° with superb registration and almost no defects has also been demonstrated [93]. Fig. 7

illustrates schematically how directed template self-assembly can be generated using electron beam patterns.

2.6. Scanning probe lithography

In scanning probe lithography (SPL), several techniques including scanning tunneling microscopy (STM), atomic force microscope (AFM), or near-field scanning optical microscopy (NSOM) may be employed to pattern nanometer-scale features. Scanning probe lithography allows manipulation at the molecular level and in parallel for the mapping of surface topography with atomic resolution [2,5–8,116–140].

SPL techniques such as AFM, STM, and NSOM are commercially available tools for nanofabrication. They are capable of nanoscale registration. The process of SPL involves deposition of molecules onto various surfaces in a certain arrangement and their imaging usually by a serial patterning method. However, it is a low throughput process. Further development of these tools could pave the way for patterning large areas in manufacturing. One established SPL approach is dip-pen nanolithography (DPN), which involves depositing nanoparticles or molecules, selectively, onto a surface [2,5,141]. Fig. 8 shows a variety of nanostructural patterning using SPL techniques. For example, Fig. 8A and B shows the accomplished precise positioning of a large number of Fe atoms by using an STM tip [142,143]. The DPN process involves the use of one or several AFM tips that have been previously immersed in the solution containing the molecules that are to be transferred onto a surface. The lithography is accomplished by the transfer of the material present on the surface of the AFM tip to another surface by following a predefined pattern constructed with the scanning tip (Fig. 8C) [2]. This method allows the patterning of lateral features with dimensions of around 50 nm [6]. DPN has been used to pattern molecules that include self-assembled monolayers (SAMs) for binding oligonucleotides, proteins, and viruses [2,119–121,141,144–147]. SPL can also be used to remove previously deposited structures on a surface by force-induced patterning [2,147,131,132,148–150] (Fig. 8D). In a process referred to as “nano-shaving”, an AFM tip placed in contact with the surface is used to successfully remove SAMs (Fig. 10E) in a well-defined pattern (Fig. 8F) [2,131,151].

SPL can be employed for the chemical modification of a surface [152]. For example, the possibility of localized controlled oxidation of a material surface has been demonstrated by accurately scanning an electrically conductive AFM or STM tip over the surface (Fig. 8G) [2,150,152]. It is based on an applied electric potential between the AFM tip and the surface that results in the localized surface oxidation. This allows the generation of 50-nm wide features. It has been shown that more advanced patterning approaches based on AFM tips with a carbon nanotube probe could further decrease the width of the patterned lines down to 10 nm of SiO₂ on silicon hydride surfaces (Fig. 8H) [2,153].

The approach based on simultaneous writing patterns with multiple probes has been demonstrated for swift and parallel patterning of nanostructures for large-volume production [2,154–157]. Other developments include electric-field-induced scanning probe lithography through anodization stamping [158] using novel multifunctional tips that are more wear-resistant and can carry more ink for massively parallel nanofabrication by DPN [141,159] or using fluorocarbon resist to fabricate features as small as 27 nm on 100-μm² areas within seconds [160]. The time-consuming parallelization and scanning can be possibly improved by a novel type of plasmonic nanolithography process. This promising technique can increase by two to five orders of magnitude the final throughput as compared to what is currently possible using parallel SPL or e-beam lithography [161].

Employing scanning near-field optical lithography (SNOL) or scanning near-field photolithography (SNP) can help circumvent the diffraction limit faced by conventional photolithography [140,162]. The approach employs a scanning near-field optical microscope (SNOM),

where the sample is irradiated by UV through a small (~50 nm) aperture in the near-field regime (10–15 nm) [163]. This results in the sample's exposure to non-diffracting, evanescent light emerging from the aperture that induces photo-exposure on the nanometer scale. Such selectively photo-oxidized adsorbates enable the fabrication of structures significantly smaller than the conventional diffraction limit [163]. Combining SNP with a mild etching solution (mercaptoethylamine 'MEA'), it is possible to fabricate a trench with a resolution of 1/30 (9 nm) in gold (Fig. 9) [164]. It also photochemically converts the surface chemistry of chloromethylphenylsiloxane (chlorine terminated) to a carboxylic acid [162,164].

An extension of the SNOM technique is an apertureless scanning near-field optical microscopy (aSNOM) [163,164]. In aSNOM, large, localized light intensities are achieved by local enhancement of far-field light through a nanometer-sized, pointed probe [165]. The technique aSNOM offers a significant increase in the optical resolution (~20 to 50 nm) over other photolithographic approaches. However, it is a relatively technically demanding technique [163].

A combination of SPL and either wet chemical or reactive ion etching has been developed. The method has been applied as a route for the construction of nanoimprinting molds [166]. The process employs local oxidation using AFM tips and the selective etching of Si while using SiO₂ nanopatterns as masks. Since this approach avoids the diffraction consequences of UV lithography, an extremely high resolution can be obtained at the end of the process [166]. Furthermore, I. Choi et al., have reported that combining SPL with wet chemical etching could lead to the fabrication of hierarchical silicon [167]. Hierarchical nano-terraced structures were obtained using controlled probe oxidation followed by silicon wet chemical etching by employing pre-designed fabrication schemes [167].

3. Bottom-up nanofabrication methods

Self-organizing functional systems and devices are the ultimate aim of bottom-up fabrication. Bottom-up nanofabrication approaches are related to the construction of multifunctional nanostructural materials and devices by the self-assembly of atoms or molecules. This methodology has the potential of generating functional multi-component devices by the controlled assembly of atoms and molecules, without waste or the need for making or eliminating parts of the final system. Some major technological challenges still remain to be solved, which include the surface preparation and conditioning for the controlled deposition of the atoms, control of impurities and site uniformity, quality of the reactants, etc. Some of the most prominent bottom-up nanofabrication methods are described in this section.

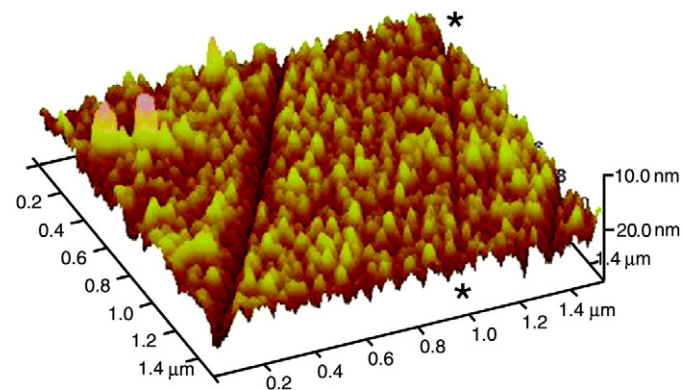


Fig. 9. An AFM image of a single trench, fwhm = 30 nm, etched into gold using a combination of SNP and the MEA etch. A 9 nm wide structure runs between the asterisks. Fig. reproduced from Ref. [164] with kind permission, © American Chemical Society.

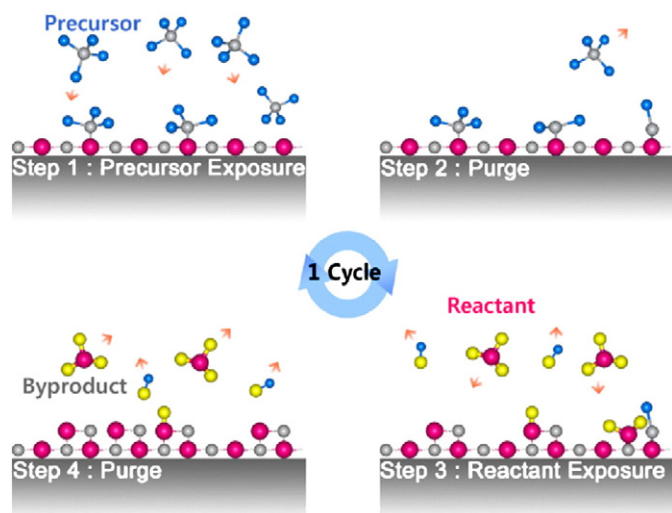


Fig. 10. Schematic illustration of the growth process of ALD. Initially, a monolayer of precursor molecules is formed on the substrate (Step 1). Inert gas purging then removes the excess of precursor 1 (Step 2). The added precursor 2 reacts with precursor 1 and forms a layer of the desired material (Step 3). Purging removes the excess of precursor 2 and reaction by-products (Step 4). The desired thickness is achieved by repeating the process. Fig. reproduced from Ref. [175] with kind permission, © Elsevier.

3.1. Atomic layer deposition

Atomic layer epitaxy (ALE) or atomic layer deposition (ALD) technique was first developed by Suntola and Antson [168]. Recently, ALD has emerged as a major potential technology for the processing and surface engineering of highly complex nanomaterials. The major advantages of using ALD include the excellent ability to control the thickness of the deposited layer which enables new approaches to modify the physico-chemical surface properties of the nanosized materials and provide opportunities for new synthesis routes to novel

nanostructures and devices [168–175]. ALD is based on sequential self-terminating surface reactions of gaseous precursors producing extremely thin, high-quality, conformal films with thickness control on the atomic level. Fig. 10 illustrates the operation of ALD [175].

ALD can be used to produce core-shell nanostructures. It has proven to be an effective nanofabrication technique for generating core-shell and shell-hollowed nanomorphologies with the desired properties. For example, ALD allows controlled synthesis of crystalline surface morphologies of core-shell nanoscale complex structures that may provide enhanced properties sought after in many applications including chemical nanoreactors, enhanced emission, controlled drug delivery, optical transmission, etc. [174,175]. Using ALD, a crystalline ZnO-Al₂O₃ core-shell nanowire structure was fabricated at a low temperature (100 °C) [176]. SnO₂-ZnO core-shell nanofibers were synthesized via a two-step process of electrospinning and ALD for gas-sensing applications [177]. In another work, a highly controllable two-step approach that combined the thermal evaporation of Bi₂O₃ with the ALD of ZnO was employed to produce Bi₂O₃-core/ZnO-shell nanostructures with highly uniform film thicknesses [178].

ALD has been applied to produce nanoengineered materials for drug delivery scaffolds. The properties of noncytotoxicity, chemical stability, and easy and versatile surface-functionalization of TiO₂ make it a promising candidate as a delivery scaffold for drugs and imaging agents [179–181]. However, to be able to act as an efficient delivery scaffold, nanoengineering of the TiO₂ scaffold surface is required to offer a means to enhance the drug delivery efficiency and imaging agents. In a recent work, controlled ALD was employed to produce a nanostructured TiO₂ scaffold surface using a spherically shaped protein cage (apoferritin) as template. The joint effects of the thermal action coupled with the osmotic dehydration were found to provide a highly uniform deposition on the outer and inner surfaces of apoferritin, leading to both hollow and core-shell nanoparticles depending upon experimental conditions (Fig. 11) [182].

ALD has also been employed for mass production of one-dimensional (1D) nanostructures. They are primarily produced by using highly porous materials such as aerogel or anodized aluminum

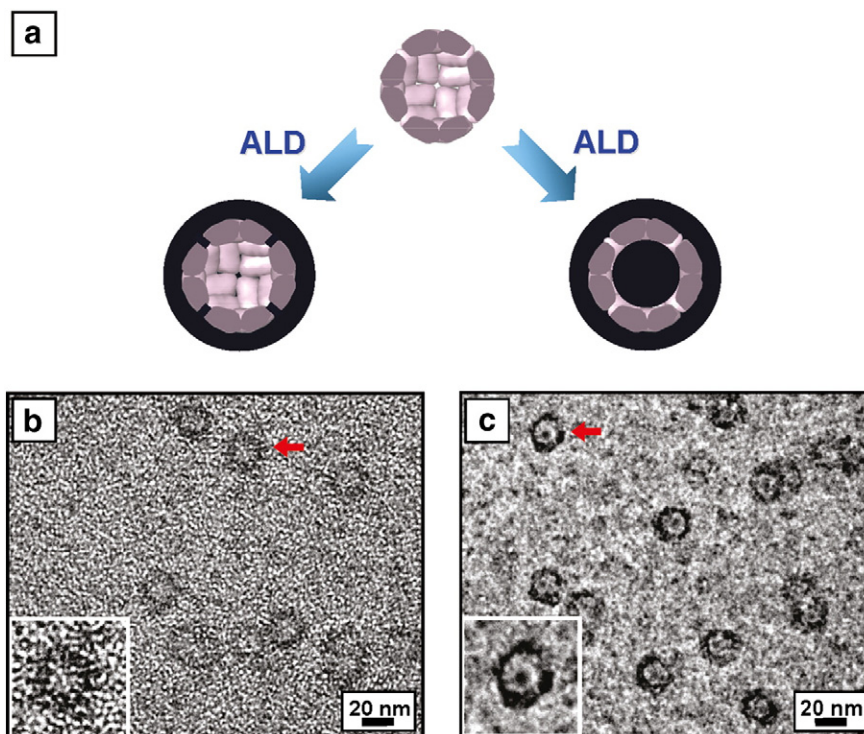


Fig. 11. (a) Schematic depiction of two different TiO₂ nanostructures obtained by the ALD process. Typical bright-field TEM images of (b) hollow shell and (c) core-shell nanoparticles templated by apoferritin. Fig. reproduced from Ref. [182] with kind permission, © American Chemical Society.

oxide (AAO). Materials with 1D characteristics can be obtained by ALD by completely filling the holes of such porous materials with various aspect ratios. This approach can be extended to a large variety of materials, such as metals, semiconductors, or oxides, to produce 1D structures with excellent conformity and gap-fill abilities [175].

Among other porous materials, AAO with high aspect ratio nanoholes or nanopores has been widely used as a nanotemplate for nanofabrication of 1D nanostructures by ALD. Recent examples include the fabrication of catalytically active membranes through the deposition by ALD of AAO and Al_2O_3 to lower the nanoholes' size to 10 nm, followed by the successive deposition of $\text{V}_2\text{O}_5/\text{H}_2\text{O}_2$ that act as the catalytically active system [183], the formation of photoanodes of high efficiency by coating ZnO over AAO membranes through ALD, and/or the controlled positioning of ZnO and V_2O_5 stripes [184,185]. Other applications include the deposition of nano TiO_2 photocatalysis on AAO membranes or Ni nanowires [186], stand alone ZnO–ZnS core-shell nanotubes or TiO_2 nanotubes [187,188], deposition of ferromagnetic nanotubes made out of Co and Ni in AAO [189], Fe_3O_4 nanotubes with high coercive magnetic fields for high-density data storage applications [190], ZnO nanorods with enhanced field emission characteristics [191], ALD SiO_2 using AAO/Si [192], and fabrication of Ru nanostructures using ALD of Ru [193]. Porous nanocomposite materials have also been fabricated by ALD using a coating of aerogels. For example, by using very thin Al_2O_3 ALD films, ALD ZnO was deposited on a silica aerogel monolith [194], metallic nanoporous structures using ALD W on carbon, alumina and Germania aerogels [195,196], and also nanoparticles of Ru deposited on the aerogel surface [175,197].

The use of ALD along with different self-assembly processes and structures is a promising approach to create arrays of nanostructures of high periodicity without using expensive lithography approaches [175,198]. Self-assembling diblock copolymers have been used in combination with ALD to fabricate metal oxide capacitors with enhanced storage ability [199], hollow inorganic nanospheres and nanotubes on nanosize polymer units [200], Polystyrene (PS) with embedded Ag nanostructures as plasmon resonance sensors [201], and a nanobowl array using (PS) nanospheres and low temperature TiO_2 ALD [175,201]. Other examples of nanofabrication using combined ALD and self-assembly are the construction of inverse opal photonic crystals [175,202–210] and self-assembled monolayer-based nanofabrications [211–227].

ALD has also been demonstrated for nanoscale device fabrication [175,228]. Interesting examples are the processing of ultra thin photovoltaic devices in which p-type CuInS_2 was introduced inside the porous structure of the n-type TiO_2 [170,229], [297], functionalization of single-walled carbon nanotubes by DNA used for the improved growth of HfO_2 oxides by ALD [230], high-mobility, field-effect transistors (FET) and FETs with 1D channel materials [231–234], non-volatile memory devices [235–238] etc.

3.2. Sol–gel nanofabrication

Sol–gel processing has been widely implemented for the fabrication of nanostructured functional metal oxide materials and alloys. Compared to physical, chemical, and plasma deposition techniques, sol–gel processing is very cost-effective. The sol–gel process relies on a combination of primarily metal precursors in solution and deposition of the precursors on suitable substrates and subsequent heat treatment to cause oxidation and/or sintering of the final products. Recently, much interest has been focused on the sol–gel synthesis of materials based on the hydrolysis and condensation of molecular precursors for the growth of a wide range of inorganic materials. Sandhage and co-workers [239] have reported a continuous nanocrystalline rutile TiO_2 -based coating on butterfly templates by the sol–gel technique. The replica retains both the macro- and microstructure of the organic tissue. Therefore, the preparation principle through sol–gel synthesis of inorganic materials inspires us to accept the challenge of constructing layered double hydroxides (LDHs). LDHs, also well-known as hydrotalcite-like compounds or anionic clays, are inorganic layered materials that are extremely interesting due to their possible applications in catalysis, adsorption, separation, sensors, electrochemistry, and bionanotechnology. Their general formula is expressed by $[\text{M}^{\text{II}}_{1-x}\text{M}^{\text{III}}_x(\text{OH})_2](\text{A}^{n-})_{x/n}\cdot m\text{H}_2\text{O}$ (M^{II} divalent and M^{III} trivalent metals, respectively, A^{n-} n -valent anion). Zhao et al. fabricated hierarchical films of layered double hydroxides by using a sol–gel process and tested their high adaptability in water treatment [240]. Fig. 12 shows the nanostructured coatings of NiAl–LDH on ordinary copier paper.

They also demonstrated that these metal(II)Aluminum LDH alloy films with various morphologies and hierarchical structures show strong adsorption capability for dye molecules (sulfurhodamine B and Congo red) and Cr(VI) ion in water. Therefore, sol–gel

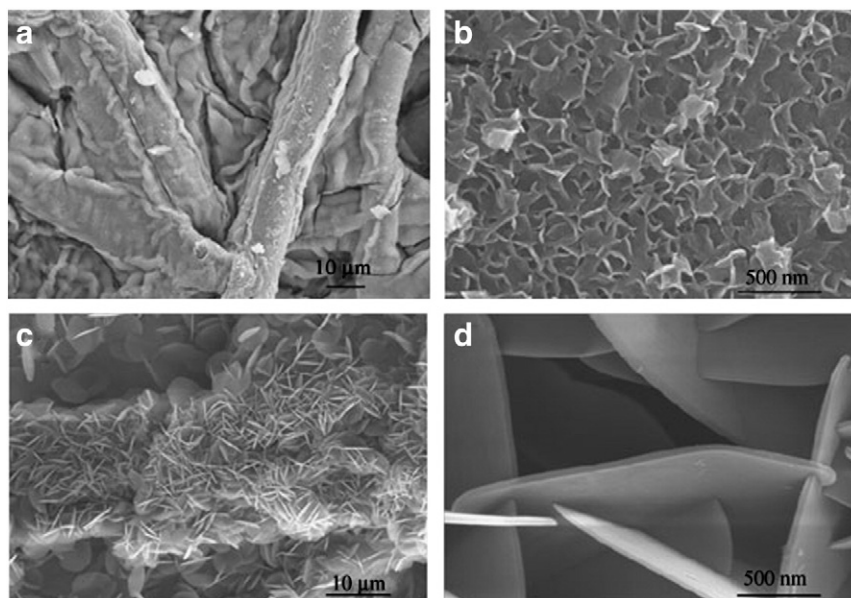


Fig. 12. SEM images of the NiAl–LDH/paper film obtained at (a) low magnification and (b) high magnification. SEM images of The MgAl–LDH/paper film at (c) low magnification and (d) high magnification. Fig. reproduced from Ref. [240] with kind permission, © The Royal Society of Chemistry.

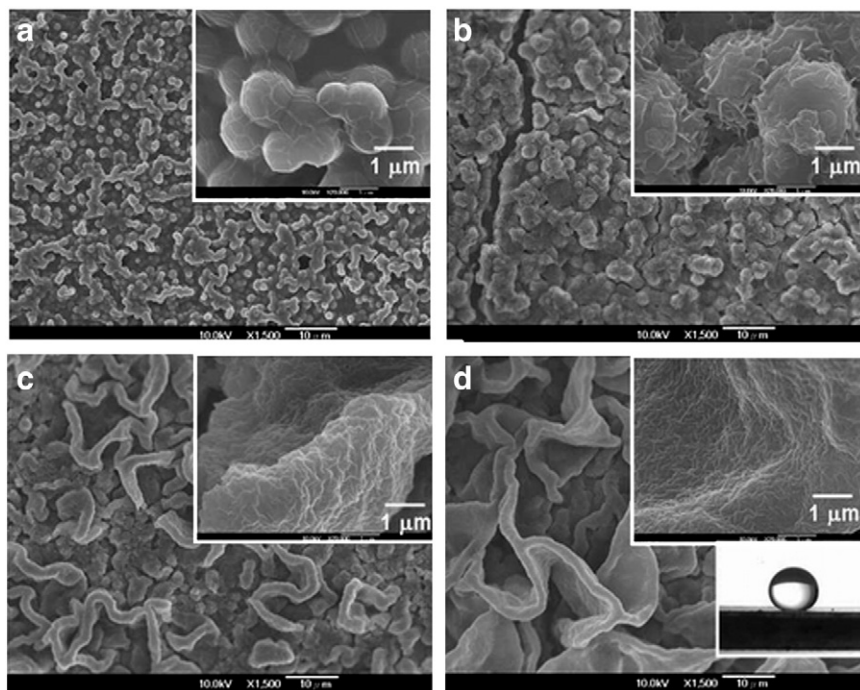


Fig. 13. Spin coating of (a) 1.5, (b) 20, (c) 30, and (d) 50 wt.% DTS solution on top of the second layer of SiO_2 particles. Fig. reproduced from Ref. [243] with kind permission, © American Chemical Society.

synthesized nanostructured thin films of metal alloys offer new possibilities for the rational design and fabrication of hierarchical LDH films, which could potentially be applied in the fields of catalysts, adsorbents, and membrane separation.

Another common application of sol-gel nanostructured thin films is the utilization of nanoparticles such as silica generated by the sol-gel process to form highly liquid repellent (superhydrophobic) surfaces and films. For this method, in general, there are two routes to construct the superhydrophobic surface. One is to create a rough

surface by aggregation or assembly of the silica particles through dip coating, spin coating, spraying, or layer-by-layer technique followed by chemical surface modification [241]. The other is to produce the hydrophobic silica or silica composite nanoparticles during the sol-gel process by adding alkylsilane or fluoroalkylsilane reagents, followed by dip coating, spin coating, or spraying to create the surface roughness [241,242]. An alternative procedure has been recently proposed [243] to construct a superhydrophobic surface on polydimethylsiloxane (PDMS), i.e., a vapor-liquid sol-gel process in

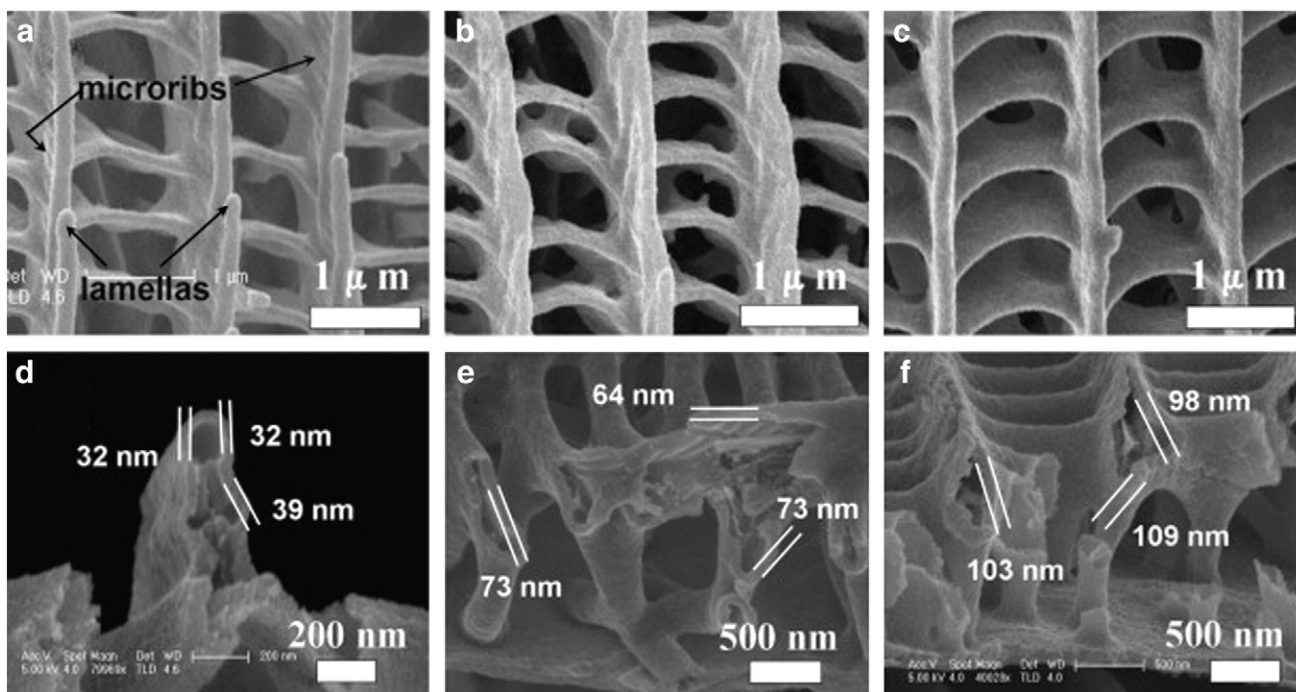


Fig. 14. Sol-gel technique for the fabrication of well-organized hierarchical SnO_2 structures with controlled wall dimensions. Field emission scanning electron microscope images of the biomorphic SnO_2 : (a and d) 30–40 nm for SnO_2 -1, (b and e) 60–80 nm for SnO_2 -2, and (c and f) 90–110 nm for SnO_2 -3. Fig. reproduced from Ref. [247] with kind permission, © Elsevier.

conjunction with spin coating. Spin coating of the reactant is performed prior to the vapor–liquid sol–gel process, during which the reaction takes place directly at the surface of the PDMS substrate instead of occurring in the bulk solution as in the conventional sol–gel process. By forming two layers of SiO_2 particles and spin coating the dodecyltrichlorosilane (DTS) solution, a superhydrophobic surface is obtained on the PDMS substrate as shown in Fig. 13. Superhydrophobic coating technology has the potential of being scaled up and to be used for the generation of surfaces with tunable surface energies that could mitigate water deposition and ice formation. This task is still extremely challenging given the fact that up to date there is still no universally accepted solution for the mitigation of ice formation and buildup with major economic implications. The complete solution requires a combination of nano and micro-scaled roughness with the alteration of the surface energy of the substrate.

By forming two layers of SiO_2 particles via vapor–liquid sol–gel process in conjunction with spin-coating of 50 wt.% or more DTS solution, a complete coverage of the wrinkle-like structure on the PDMS surface was obtained, rendering the surface superhydrophobic with a 162° static contact angle, less than 5° contact angle hysteresis, and 2° sliding angle. Two layers of SiO_2 particles are required to allow the hydrophobic oligomeric siloxane to form the wrinkle-like structure when spin coating the DTS solution at a concentration larger than 30 wt.%. With such a technique, various substrates bonded to the modified PDMS can render themselves superhydrophobic which could have unique biomedical applications [243].

Similarly, nanostructured metal oxides can be fabricated using biomimetic sol–gel routes for novel gas sensors. For example, SnO_2 with the wide bandgap of 3.62 eV is an intensively studied semiconducting metal oxide (n-type) with significant gas-sensing applications [244]. Sandhage and co-workers have previously presented interesting data showing that silica coated with either silicon or SnO_2 and which presents 3D hierarchical porosities of diatoms has superb NO detection capabilities [245].

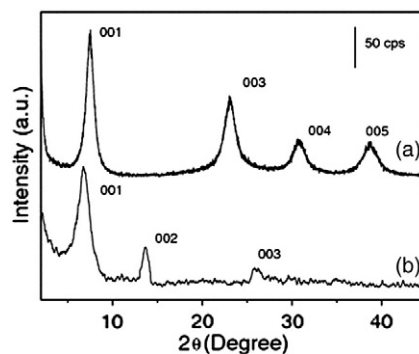


Fig. 16. X-ray diffraction patterns of the samples: a V_2O_5 xerogel and b calcined mesostructured V_2O_5 . Fig. reproduced from Ref. [248] with kind permission, © Springer.

Ordered macroporous SnO_2 structures with various pore sizes and opal/inverse opal type, as well as controllable necking, have been fabricated. Furthermore, the 3D hierarchical arrangement is an important characteristic for gas sensing applications [246]. Since most butterfly wings have excellent 3D hierarchical porous architectures, Song et al. [247] used them as templates for the SnO_2 fabrication replicas with highly adjustable wall thickness and morphologies (Fig. 14) [247].

The wall thickness can be easily adjusted by varying the overall concentration levels of the impregnants or the length of the immersion process. Given the ability to control the size of the grains as well as the organization of the porous 3D hierarchies, biomorphic SnO_2 has excellent sensing properties for ethanol and formaldehyde as shown by Song et al. [247]. Most noticeably, the sensing response of the SnO_2 nanostructures increased when the thickness of the walls decreased (Fig. 15) [247].

Sol–gel technologies also offer very unique opportunities for the synthesis of new classes of energy storage materials and alloys. The vanadium pentoxide xerogel ($\text{V}_2\text{O}_5 \cdot n\text{H}_2\text{O}$) matrix, for example, has been

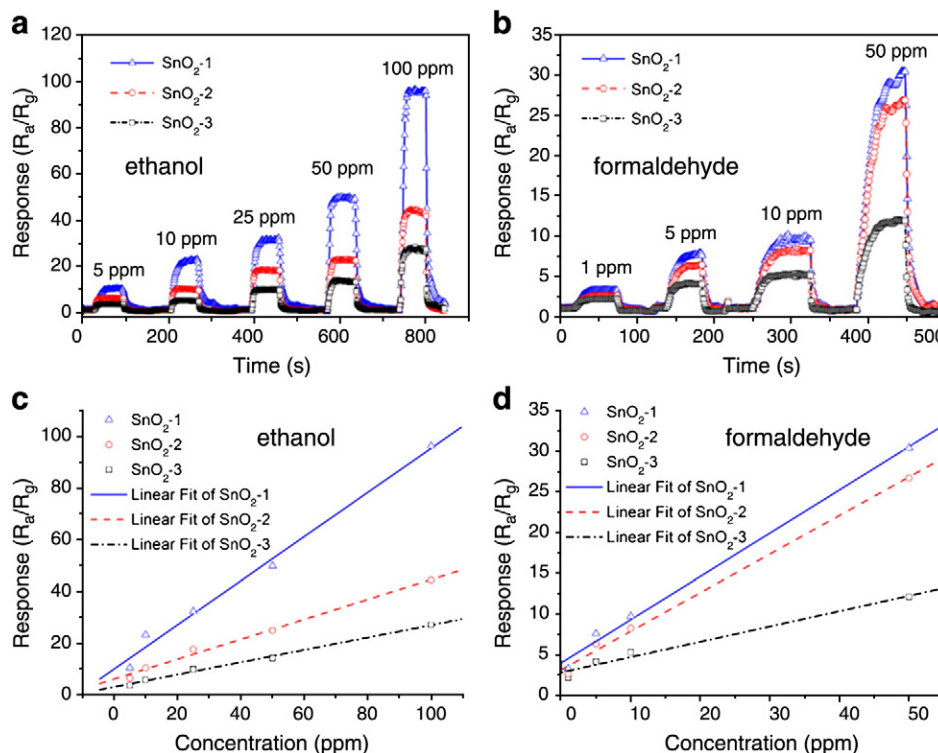


Fig. 15. (a and b) Real-time sensing responses and (c and d) response variations of the sensors to ethanol (170°C) and formaldehyde (210°C) of different concentrations, respectively. Fig. reproduced from Ref. [247] with kind permission, © Elsevier.

investigated as a host material [248]. $V_2O_5 \cdot nH_2O$ has excellent electrochemical properties and both ionic-electronic conduction. The V_2O_5 films have been employed because they have the ability to release or to store significant levels of energy during Li^+ intercalation/deintercalation in lithium-ion batteries. Furthermore, it is possible to produce highly porous V_2O_5 by sol-gel routes. The large surface area of porous V_2O_5 films allows effective penetration of the electrolyte in its structure. Such a process can enhance the kinetic performance of the batteries by reducing the ionic paths. E. Guerra et al. successfully prepared porous gel vanadium pentoxide ($V_2O_5 \cdot nH_2O$) by using sodium metavanadate ($NaVO_3$, 99%) and the ion-exchange approach [248].

Fig. 16 shows the X-ray diffraction spectra of the $V_2O_5 \cdot nH_2O$ gel structures and of the calcined mesostructured V_2O_5 . The diffraction patterns of the V_2O_5 materials have rather broad peaks, indicating a low crystallinity, but with the V_2O_5 xerogel presenting a higher crystallinity in comparison with the calcined V_2O_5 . Fig. 19 presents SEM analysis of the V_2O_5 xerogel and the calcined mesostructured V_2O_5 , indicating the surface morphological changes that took place in these samples. The hydrated vanadium pentoxide structures (Fig. 17a) show the presence of a randomly oriented network of interconnected chains. However, the calcined mesostructured V_2O_5 (Fig. 17 b, c) shows a highly porous surface, characteristic of the mesoporous materials. This type of structure enables ion impregnation and the effective operation of an energy storage device such as a battery. Cyclic voltamograms taken from such mesoporous oxides

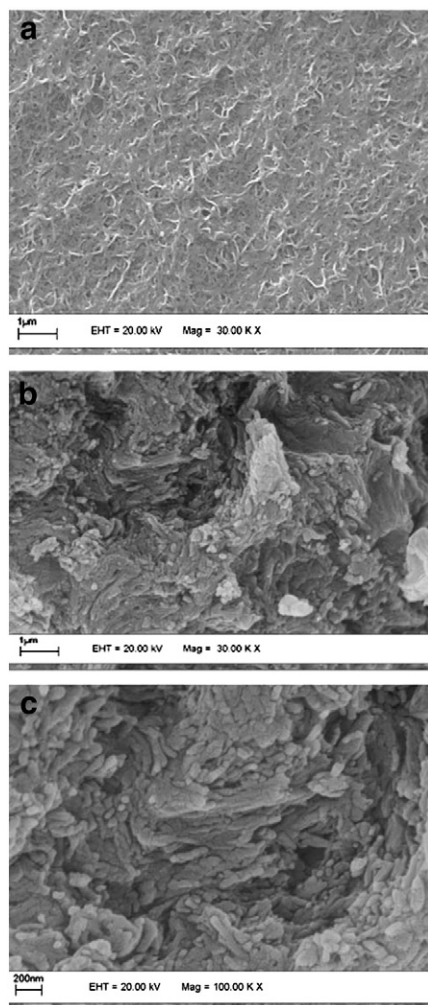


Fig. 17. Scanning electron micrographs of (a) vanadium pentoxide xerogel (b) calcined mesostructured V_2O_5 in $\times 0,000$, and (c) calcined mesostructured V_2O_5 in $\times 100,000$. Fig. reproduced from Ref. [248] with kind permission, © Springer.

indicate that the pore formation in the structure of the materials is associated with an increase in the number of active sites, allowing Li^+ ions to penetrate more deeply into the material and to have better diffusion. Furthermore, the volumetric changes that were observed after several steps of insertion/deinsertion of Li^+ ions are reflected in irreversible modification in the V_2O_5 structures. Without the presence of the porous structure, the high activity of the oxide most probably would have been lost, therefore indicating that the highly porous material is a superior choice as the cathodic material for Li^+ batteries [248].

3.3. Molecular self assembly

Molecular self-assembly (MSA) is the process by which molecules assemble themselves without the presence of outside interactions [249–251]. Self-assembly in nature often takes place spontaneously. A typical example is the formation of the lipid bilayer of the membranes of cells. MSA can be leveraged to imitate these strategies that are present in nature for the creation of new types of molecular systems that can self-assemble to form supramolecular assemblies. MSA is a promising approach that can be applied to control the types and the intensity of the intermolecular forces between these molecular systems. This could result in the formation of previously unachieved nanomaterials [252]. However, given the many complex examples observed in nature, MSA is basically an experimental approach that is still not completely understood. This is due to the fact that most of molecular assemblies present a high degree of complexity and are difficult to isolate individually [252].

The approach based on Self Assembled Monolayers (SAMs) corresponds to the most versatile and prominent MSA strategy that has received a high degree of scrutiny and research. To form SAMs, the most commonly used molecules are the thiols and silanes [252]. For SAMs, the basic building blocks are built through chemical approaches, and they are bound together by weaker Van der Waals forces to form various structures. Due to the presence of these weak forces, it is possible to obtain reversible solution processing of SAMs allowing mass production of various nanostructural materials/systems (nanowires, electronic nanocomponents, sensors, etc.) on a large scale at a low cost. MSA has been applied in biotechnology to create molecular nanostructures for various biomedical applications. For example, the triple-helical structure of collagen peptides has recently been harnessed as a subunit in the higher-order assembly of unique biomaterials. Specific assembly signals have been designed within collagen peptides, including hydrophobic groups, electrostatic interactions, and metal-ligand binding. In this way, a range of novel assemblies have been obtained, including nano- to microscale fibers, gels, spheres, and meshes, each with the potential for novel biological applications in drug delivery, tissue engineering, and regenerative medicine [249–253].

Some of the earliest methods for generating synthetic collagen fibers from small collagen peptides involved chemical cross-linking of the peptide termini into nonreversible collagen systems [253]. For instance, (Pro-Hyp-Gly)₁₀ units were synthesized and cross-linked via amide bond-forming reactions [254]. This process resulted in high-molecular weight products composed of more than 10 linked peptide chains with nanofiber-like structures that were longer than the aggregates of (POG)₁₀ [253,254]. Alternatively, Hartgerink and co-workers used native chemical ligation to polymerize small collagen fragments (Fig. 18) [253,255]. This was achieved by placing a cysteine at the N-terminus and a thioester at the C-terminus of a (Pro-Hyp-Gly)₉ sequence. The resulting native chemical ligation led to the generation of long nanofibers with diameters of 10–20 nm. These examples indicated that small collagen fragments could assemble into fibers that mimic the diameter of natural collagen fibrils. Cell adhesion sequences were also incorporated into these synthetic collagen

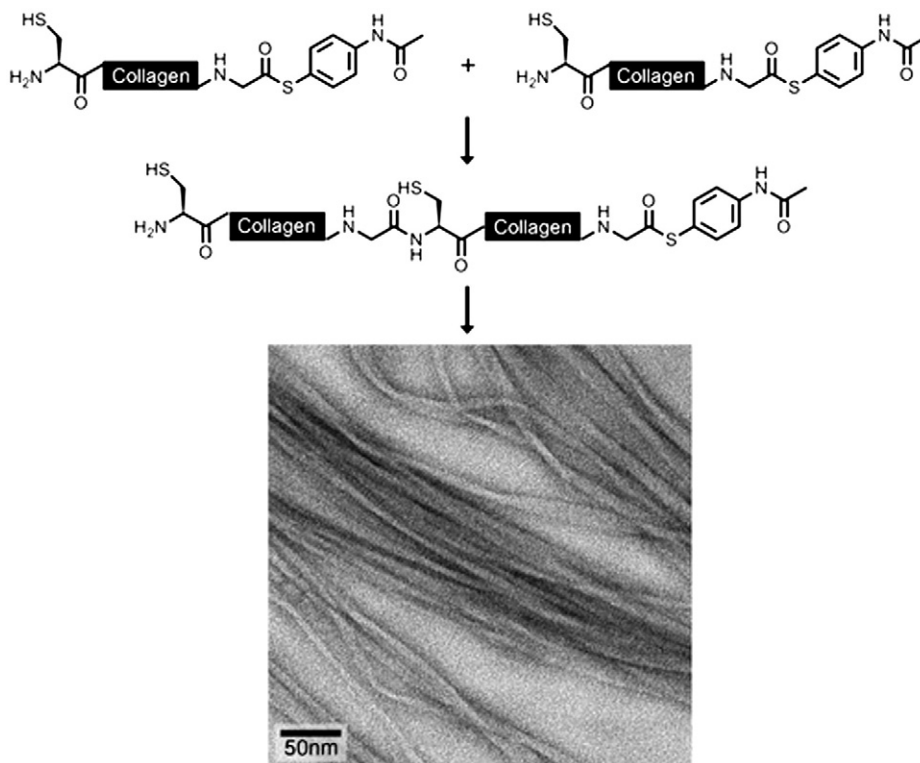


Fig. 18. Native chemical ligation of short collagen sequences into collagen fibrils. Fig. reproduced from Ref. [253] with kind permission, © American Chemical Society.

assemblies, a key feature in generating collagen materials with cell binding activities.

A sticky end organic molecular assembly approach has also been described in another MSA strategy that relies on hydrophobic, non-covalent interactions to promote collagen peptide assembly. Maryanoff and co-workers, for instance, designed a creative collagen peptide assembly strategy that relied on hydrophobic interactions from terminally placed aromatic residues [256]. Specifically, a pentafluorophenylalanine residue was placed at the N-terminus and a Phe residue added to the C-terminus of a (Pro-Hyp-Gly)₁₀ sequence (Fig. 19A). The spontaneous association of triple helices of this collagen peptide generated fibrils that were micrometers in length and resembled collagen fibers formed in murine aortic tissue, although the

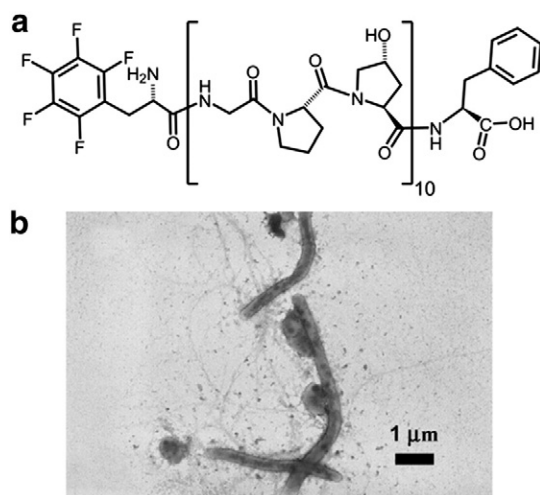


Fig. 19. (a) Sequence of a self-assembling collagen peptide with hydrophobic termini. (b) A typical transmission electron microscope image of assembled collagen fibers. Fig. reproduced from Ref. [253] with kind permission, © American Chemical Society.

assembled fibrils are significantly thicker (250 nm vs. 50 nm) (see Fig. 19B) [253].

An interesting application example of MSA is described by Kim et al., who have shown that the formation of assemblies of amphiphilic polyelectrolytes introduced within the aluminosilicate nanoplates has the potential to generate films that could act as hydrophobic barriers [257]. Approximately 100 nm-thick hydrophobic barriers produced by this approach were shown to efficiently block moisture transportation

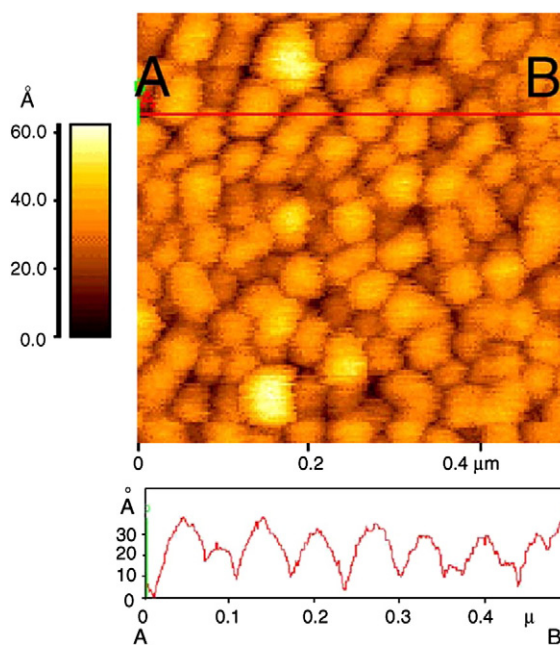


Fig. 20. An AFM image of PEPy-C18 polymers deposited on the mica substrate from the methanol solution. The samples for AFM were prepared by dipping the mica substrate into the methanol solution of the PEPy-C18 polymer for 10 s, followed by washing and drying. Fig. reproduced from Ref. [257] with kind permission, © Elsevier.

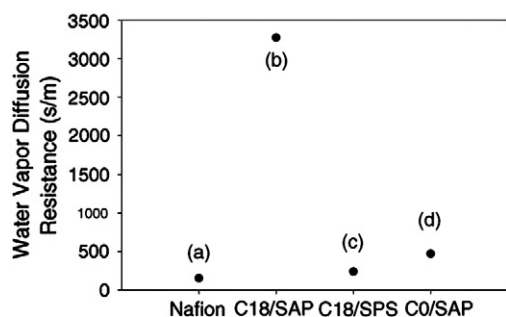


Fig. 21. Curves showing water vapor diffusion resistance of (a) pristine Nafion substrate, (b) 10-bilayer film of PEPy-C18 and saponite, (c) 10-bilayer film of PEPy-C18 and sulfonated polystyrene (SPS) and (d) 10-bilayer film of PEPy-C0 and saponite on the Nafion substrate. Fig. reproduced from Ref. [257] with kind permission, © Elsevier.

and to improve the water vapor barrier characteristics of a Nafion membrane, ca. 50 μm by up to 22 times [257]. Kim's group further produced, through the spontaneous polymerization of 2-ethynylpyridine, an amphiphilic polyelectrolyte, [poly(Noctadecyl-*n*2-ethynylpyridinium bromide), PEPy-C18] with the help of octadecyl bromide. Fig. 20 shows that the PEPy-C18 polymer does form domains of uniform dimensions over the entire surface of the substrate [257].

The resulting nanocomposite materials showed a significant enhancement (22 times higher) for the diffusion resistance compared to the pristine Nafion surfaces (Fig. 21). Such hydrophobic barriers efficiently block water molecule transportation and hence present excellent barrier properties [257].

The molecular self-assembly approaches exemplified in this section demonstrate the possibility of using supramolecular chemistry principles to craft the size, shape, and internal structure of nanoscale objects. They deal specifically with organic molecules and their self-assembly into soft, as well as hard, nanostructures such as carbon nanotubes and metallic nanoparticles. Soft nanostructures, not the original focus of nanoscience, remain the least explored systems in terms of physical properties and value as a toolbox to assemble novel materials. In this regard, MSA could be leveraged to construct and study various soft nanostructures to gain deeper insights into their functional properties.

3.4. Vapor phase deposition of nanomaterials

Vapor phase deposition techniques are primarily divided into two categories: Chemical Vapor Deposition (CVD) and Physical Vapor

Deposition (PVD). CVD and PVD techniques are intensively used to conduct combinatorial nanomaterials research and synthesis of various carbon nano-materials. CVD essentially involves the process of dissociation of molecules of the gaseous reactants, which subsequently react chemically to form various structures when activated by heat, light, or plasma discharge. Mostly solid-state, stable products are formed as a result of the chemical reactions.

The CVD technique has been widely used to grow different types of carbon nanostructures such as single-walled, double-walled, and multi-walled carbon nanotubes and lately graphene on various substrates. This technique has been further improved by the use of radio-frequency (RF) for heat generation, with a positive effect on the morphology and crystallinity of the carbon nanostructures: more advanced control of the diameters, lower levels of non-crystalline carbon formation, and a higher efficiency of carbon conversion from the gas phase to the graphitic structures [258–263]. Although major developments were already achieved during the CVD growth of graphitic nanomaterials, still a number of technological issues remain to be understood. Some of these include the role of the various catalytic systems in the final morphology of the nanomaterials, the actual growth mechanism that controls the synthesis of nanomaterials with specific characteristics and the role that each hydrocarbon plays in this aspect. Among the methods that are used to grow carbon allotropes, still CVD is the method of choice. The careful choice of the metallic catalytic system, the carbon source, and the reaction conditions are of the utmost importance [262–265].

Once the hydrocarbon decomposes, typically at high temperatures (up to 1000 $^{\circ}\text{C}$), the carbon atoms diffuse into metal nanoparticles rearranging themselves in a particular carbon network and finally precipitating out in the shape of the carbon nanostructures. The termination of carbon nanotube growth occurs when the surface of the catalyst nanoparticle is covered by amorphous carbon and the carbon atoms cannot further diffuse into metal nanoclusters [264]. There are several methods to synthesize carbon nanotubes, but the CVD technique has many advantages. This is a relatively low-cost technique that can be scaled up for the production of large quantities of nanotubes. Biris' group has also demonstrated that, during CVD synthesis, the morphological properties of carbon nanotubes can be controlled by adjusting the reaction parameters—such as the type of hydrocarbon, reaction temperature, the flow rate of the gases, and the composition of catalytic system [258,265].

We will restrict our discussions on CVD of carbon nanotubes as there are recent comprehensive reviews published on different forms of CVD

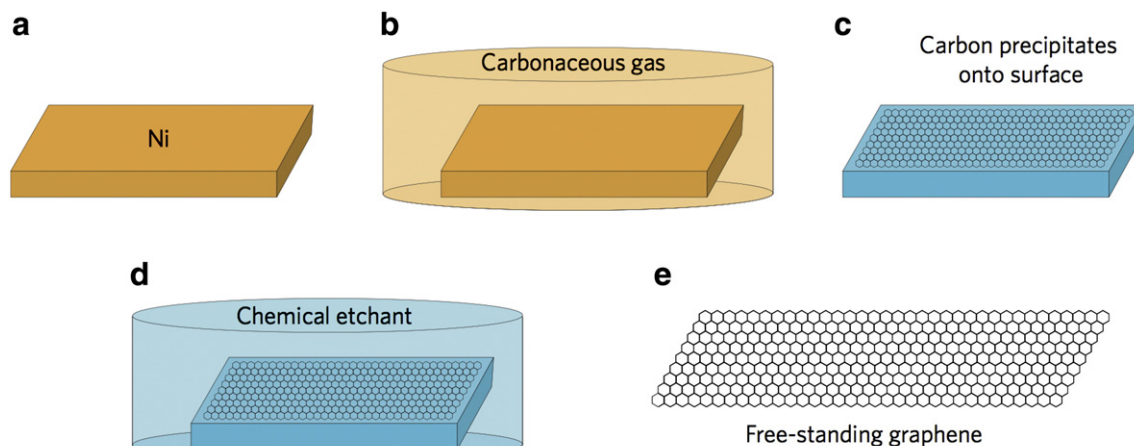


Fig. 22. Schematic illustration of the CVD process for graphene production. (a) A thin layer of nickel (Ni) is first deposited onto a substrate. (b) The Ni layer is then heated to about 1000 $^{\circ}\text{C}$ and subsequently exposed to an environment of carbonaceous gas. (c) As a result, the carbon atoms that are generated at the Ni surface diffuse into the metal. (d) The cooling of nickel results in the precipitation of carbon atoms out of the nickel layer that eventually forms graphene on the (111) faces of Ni crystallites surface. (e) A chemical etching results in the detached graphene membrane from the Ni layer. The resulting free-standing graphene layer is finally transferred onto appropriate substrates. The orange and blue colors illustrate hot and cold temperature conditions respectively. The orange and blue colors also represent different chemical compositions such as gas and chemical etchant respectively. Fig. reproduced from Ref. [303] with kind permission, © Nature Publishing Group.

and the growth of carbon nanotubes [264,266–268]. Instead, we will focus our discussion on recent developments in the CVD synthesis of another wonder carbon nanomaterial, graphene. Graphene is rapidly emerging as a material with novel properties that can be successfully used in many advanced applications in a variety of areas: electronics, gas sensors, batteries, optics, nano-structured display devices and photonics, and biomedical sectors [269–278].

Graphene is comprised of a single-layer of sp^2 -hybridized carbon atoms, arranged hexagonally in a two-dimensional sheet. It was isolated for the first time in a free-standing form out of graphite in 2004 [279,280]. Since then it has become a very active area of research and has garnered considerable interest due to its amazing electronic, electrical, mechanical and optical properties [279,281–284]. Graphene is also found to be chemically and mechanically stable and has high mobility, ballistic transport, and quantum Hall effect at room temperature making it a great candidate for nano-electronic applications [285–302].

The synthesis of high-quality and large-area (up to several centimeters square) graphene sheets with few defects and excellent electrical and optical properties is still one of the most intensively researched topics in nanotechnology [303]. Synthesis of large-scale and high-quality graphene will expand its scope in various applications. Recent advances in direct CVD synthesis of graphene have demonstrated the possibility of producing high-quality, large-area layers of graphene without sophisticated and possibly damaging mechanical and chemical procedures. Samples of large-area, single- and few-layer graphene have been manufactured by CVD and further transferred to a number of other possible substrates [304–306].

The CVD-synthesis process (Fig. 22) first involves dissolving carbon into the subsurface of a nickel film. Subsequent cooling of the nickel substrate allows the carbon to precipitate out. Adjusting the rate of the thermal cooling and the carbon concentration makes it possible to accurately control the thickness and the crystalline

ordering of the precipitated carbon. As noted by A. Obratzsov, the concentration of deposited graphitic carbon is mainly given by the following parameters: type and concentration of the carbon-containing gas, temperature and the overall thickness of the Ni film [303,304]. The resulting graphene layer can be detached from the substrate after the metal film is removed by chemical etching. Ultimately, it can be deposited or transferred onto other surfaces [303–306].

X. Wang et al. have synthesized by CVD (MgO supported Co catalyst at 1000 °C) large graphitic sheets that were substrate-free and composed of only a few layers [307]. The analysis of the resulting graphitic layers revealed the presence of localized sp^3 defects within the sp^2 carbon graphitic structure [307].

Recently, Biris' team has reported a low-cost method for the large-scale synthesis of high-quality few-layer graphene structures via radio-frequency catalytic chemical vapor deposition (RF-cCVD). RF excitation of the metallic catalytic systems is believed to improve the process of carbon uptake by the catalytically active metal clusters, and the more efficient conversion of the atomic carbon into C–C bonds and the graphitic structures. This practical and highly reproducible technique may be utilized to produce large quantities of graphene-type nanomaterials for various advanced technology applications. Few-layer graphene sheets were grown over a bimetallic catalytic system (Fe-Co/MgO) having acetylene as the carbon source [308]. Previously, the group has shown that this MgO-supported Fe-Co bimetallic catalytic system is extremely versatile, and, depending on the reaction parameters, different types of carbon nanostructures may be synthesized [309]. Furthermore, Dervishi et al. reported that by only varying the flow rate of the hydrocarbon, one can control the size and layer number of graphene sheets synthesized over the same catalytic system [310]. The RF-cCVD method significantly reduces energy consumption during synthesis while preventing the formation of undesirable types of carbons, such as amorphous and glassy carbon [311].

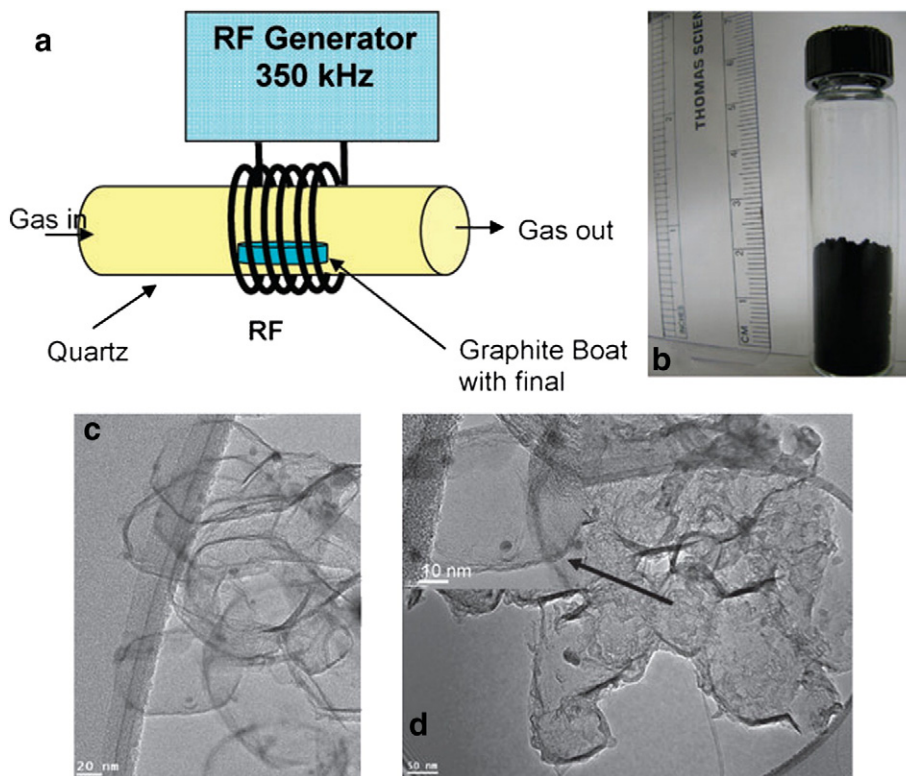


Fig. 23. (a) Schematic of the growth process for the few-layer graphene using the RF generator, (b) photograph of high-yield graphene synthesized in large quantities, (c) TEM image of few-layer graphene sheets overlaid side by side with hexagonal shape, (d) low-magnification TEM image of the graphene nanosheets deposited on top of the carbon-coated copper grid. The inset shows a high-resolution image of a few-layer graphene sheet with diameter of 100 nm. Fig. reproduced from Ref. [308] with kind permission, © The Royal Society of Chemistry.

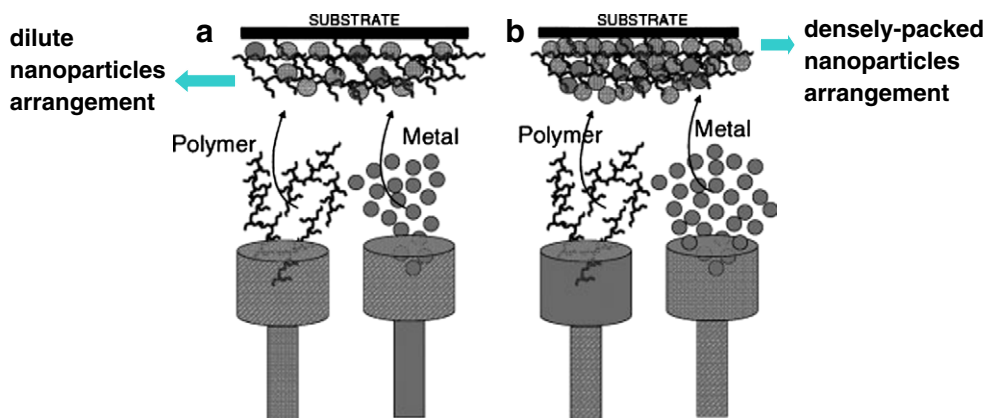


Fig. 24. Schematic representation of e-beam-assisted codeposition of polymer and metal and the deposition-parameter-dependent resulting nanostructures. Fig. reproduced from Ref. [320] with kind permission, © John Wiley.

To synthesize graphene samples, the Fe-Co/MgO catalyst system with a 2.5:2.5:95 wt% stoichiometrical composition was prepared by using the impregnation method [265]. The as-produced graphene sheets were purified with diluted HCl solution under gentle sonication. Fig. 23(a) shows a schematic diagram of the growth process for the few-layer graphene using the RF generator. Fig. 23(b) shows an optical image of the as-produced few-layer graphene sheets in large quantities. Transmission electron microscopy (TEM) analysis revealed a high-yield production of few-layer graphene structures. High- and low-resolution TEM images (Fig. 23(c) and (d)) indicated that the as-produced samples were composed of graphene sheets overlaid side by side, with dimensions of 100–110 nm in diameter [308]. The comprehensive analysis of graphene sheets (1, 2, 3 layers) is still very complex, given their unique structures and especially their thickness. Atomic force microscopy (AFM) is the method of choice, but still a series of problems needs to be addressed, such as the presence and the thickness of the dead space between the graphene layers and the substrate, the cantilever tip radius, the bending of the sheets, and the presence of substrate non-uniformities. As a result, a combination of transmission electron microscopy (TEM), AFM, and spectroscopic methods such as Raman should be used.

Among other forms of CVD for nanofabrication, focused ion beam-assisted chemical vapor deposition has been used to fabricate complex 3D nanostructures. By using a Ga precursor gas, GaN nanocrystals (200 nm × 100 nm × 50 nm) were produced while under irradiation; atomic nitrogen radicals were simultaneously introduced onto the surface. The focused ion beam had a major importance for the generation of nucleation sites and assisting the GaN nanostructures' growth [312]. Various nanostructures of ZnO (nanowires, nanobelts, nanostars, nanosprings, etc.) have been grown by metal oxide chemical vapor deposition (MOCVD) [313–315].

In PVD method, materials are evaporated by electron beam, ion beam, plasma, or laser. The evaporation material (monomers, molecules, atoms, etc.) is vaporized with the supplied energy and solidifies on the surface of the substrate. PVD processes are usually carried out in an ultra-high to high vacuum environment. This enables the vapor to reach the substrate without interacting in the reaction chamber with any other gaseous atoms.

A versatile e-beam-assisted codeposition technique to fabricate multicomponent nanomaterials has been developed and presented earlier by Biswas et al. [9]. The method allows for several materials (polymers, metal, insulators, ceramics, and semiconductors) to be simultaneously or sequentially evaporated out of metal crucibles that are bombarded by electrons. This technique allows exploration of a wide range of organic and inorganic materials with well-defined component ratios and nanoscale morphologies [9,316–322]. Fig. 24 shows a schematic representation of the codeposition process of

polymer and metal and the resulting nanostructures depending on the deposition parameters.

Using this system, Bayer et al. fabricated nanostructured composites from a variety of industrially important polymers such as poly(ethylene oxide) (PPO)/polystyrene blends with metal nanoparticles. The surface morphology and the dielectric properties of these polymer-metal composites can be controlled by using the highly porous structure of PPO polymer as shown in Fig. 25. Such polymer-silver composite thin films show appreciable capacitance density under radio frequency polarization [320].

Faupel's group has demonstrated a similar vapor phase codeposition approach to fabricate mostly polymer-metal nanostructures and nanocomposites for various functional applications [323–329]. Using co-evaporation of metal and polymer components, nanocomposites containing bimetallic $\text{Au}_x\text{Ag}_{1-x}$ and $\text{Cu}_x\text{Ag}_{1-x}$ nanoparticles in a Teflon AF matrix were produced to tune the position of the surface plasmon resonance [229]. The group also demonstrated high-density magnetic nanorods in a polymer matrix by co-evaporation of ferromagnetic Fe-Ni-Co and Teflon AF polymer. Co-evaporation of a Fe-Ni-Co alloy together with the fluoropolymer Teflon AF was shown at elevated substrate temperatures that resulted in extremely thin rods (~5 nm) with a very large aspect ratio. Such ultra-fine ferromagnetic nanorods can be obtained above a critical ratio of the metal/organic deposition rates. The growth of nanorods is attributed to a self-organization process which is based on the very low interaction energy between metal and polymer as well as on a critical threshold in the flux ratio of metal/polymer components. Above this critical threshold, the growth of the metal particles normal to the substrate is too fast to embed them into the growing polymer matrix [328,330]. Fig. 26 shows a cross-sectional transmission electron microscopy image of such a nanorod film. At low temperatures, where the condensation coefficient is large, high filling factors and growth of clusters are observed.

Furthermore, in a recent joint work, the groups of Elbahri and Faupel demonstrated an omnidirectional transparent conducting-metal-based plasmonic nanocomposite (TCM). Mady Elbahri et al. reported the first experimental realization of the omnidirectional TCM by coating a metal film on a glass substrate with a thin layer of metal/polymer nanocomposite. The design of this new optoelectronic material is based on a plasmonic metamaterial that consists of a thin metal film with a nanocomposite coating containing metal nanoparticles (Fig. 27). The omnidirectional TCM exhibited optoelectronic properties superior to indium tin oxide (ITO) that is widely used in optoelectronic devices [331]. In the present case, the nanocomposites matrix was not deposited by evaporation but by a special RF sputtering technique from a Teflon target used earlier by Biederman [332].

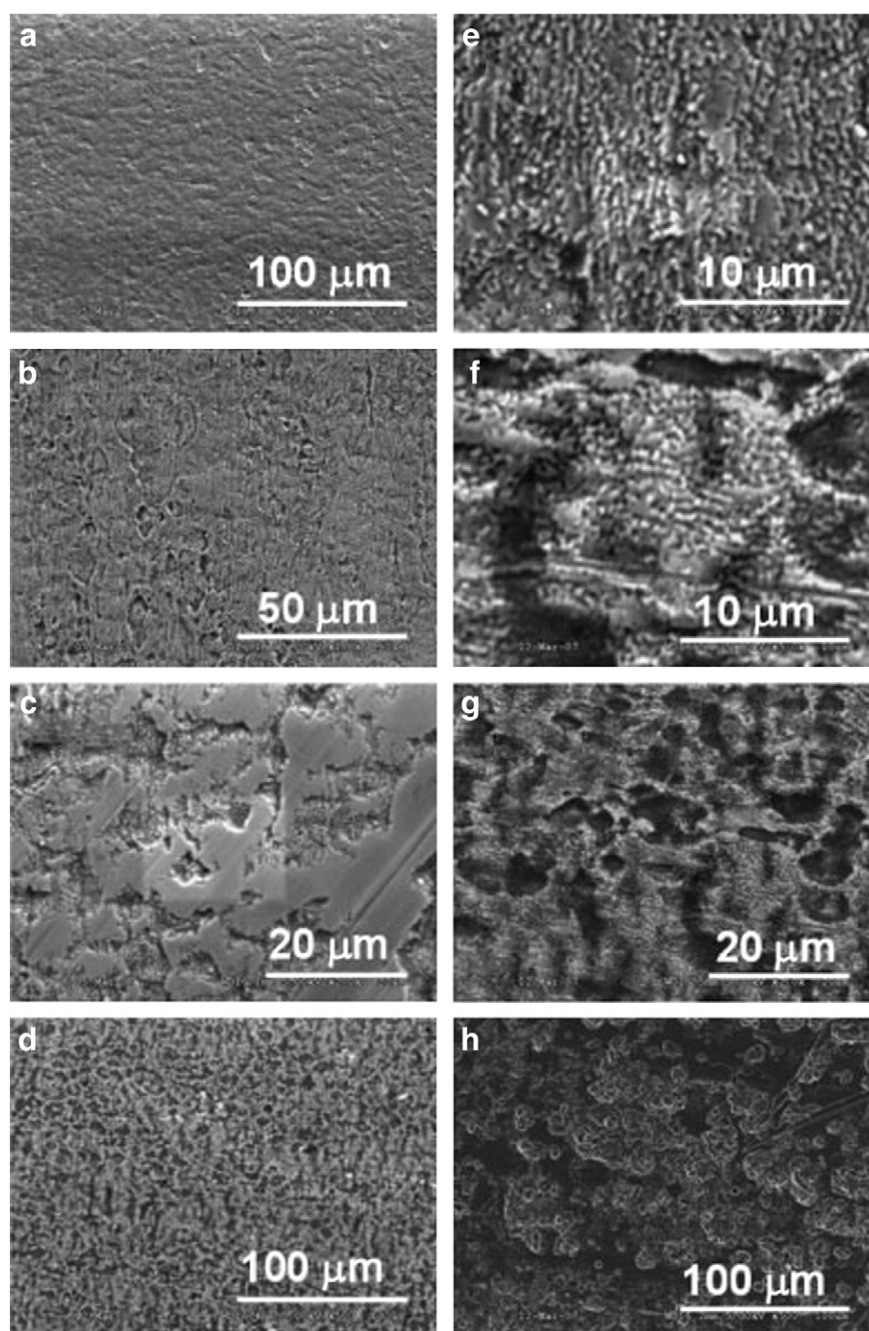


Fig. 25. SEM images showing surface morphology of various PPO/Ag composites as a function of the approximate Ag inclusion ratio. (a) 87% Ag, (b) 82% Ag, (c) 73% Ag, (d) 64% Ag, (e) 53% Ag, (f) 49% Ag, (g) 34% Ag, and (h) 21% Ag. Fig. reproduced from Ref. [320] with kind permission, © John Wiley.

3.5. DNA-scaffolding for nanoelectronics

The use of deoxyribonucleic acid (DNA), a fundamental element to all living organisms, can lead to potential applications in the fields of biology or medicine. Recently, DNA-based scaffolding has emerged a powerful nanofabrication tool. DNA-based fabrication of functional nanomaterials are covered in comprehensive reviews on DNA origami [333] DNA-templated assembly [334], self-assembly for medicine [335] and for molecular sensing [336]. Here, we outline DNA structures and highlight the recent advances in directed self-assembly and metallization of DNA for its potential applications in nanoelectronic architecture and photonics.

The DNA molecule is generally viewed as a long polymer chain formed by two single strands in the shape of twisted ladder structure

often called “double (stranded) helix”. Each single strand (short ones often called oligonucleotides) is made up of a sequence of the nucleotides in such a fashion that a phosphate group links to two sugars through a phosphodiester bond. Each rung of the ladder, called a base pair, is formed by two nitrogenous bases through hydrogen bonds following a special pairing rule, i.e. adenine (A) with thymine (T) and cytosine (C) with guanine (G). The vertical outside “backbones” for the helix are made up of the sugar and phosphate molecules, while the bases are stacked one on another at 0.34 nm spacing inside of the backbone. One complete turn contains 10 base pairs and measures 3.4 nm long and 2 nm in diameter. However, DNA also bears other complex structural forms other than the helix. A well-known example is DNA origami, in which a long single strand DNA (ssDNA) is folded by self-interaction or by interacting with multiple helper oligonucleotide

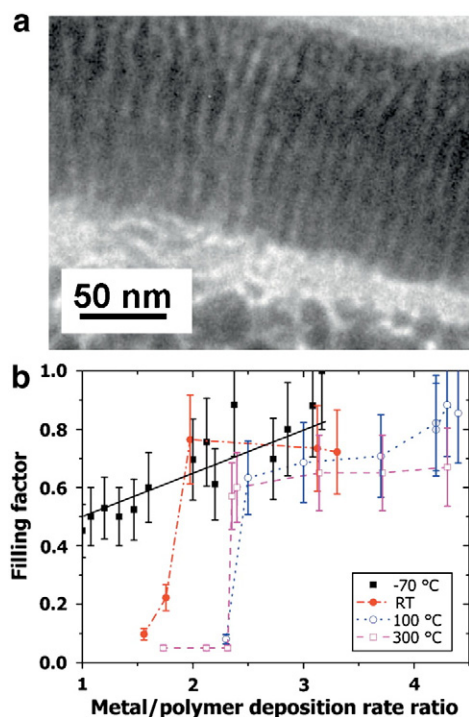


Fig. 26. (a) TEM image of Fe-Ni-Co nanorods on top of a layer of Ag clusters in an evaporated Teflon AF matrix. (b) Metal filling factor vs. metal/polymer deposition rates at various temperatures. For the lowest temperature, cluster formation is observed. Fig. reproduced from Ref. [330] with kind permission, © American Institute of Physics.

strands (also called staple strands) with a resolution ~ 6 nm [337]. These remarkable abilities in molecular recognition and structural configurations allow for DNA to self-assemble into a variety of geometries ranging from simple 2-D smiley faces [337] to many exotic 3-D shapes, e.g. boxes with lids [338] and curved 3-D hemispheres and flasks [339].

It should be noted that although individual origami can be reliably produced, but most of these self-assembly processes occur in solution phase held in tubes or containers. For implementation in nanoelectronics fabrication, it is apparent that important issues, such as the ability for controlled large-scale patterning on solid semiconductor substrates and electrical conductivity, have to be addressed.

Equivalent to nanolithography, one prerequisite is the ability to pattern ordered DNA features. Towards this end, several binding mechanisms were utilized to pattern DNA to the desired positions on a substrate that include hydrophilicity and covalent attachment. Kershner et al. [340] described a method of assembling DNA origami into complementary binding sites predefined with e-beam lithography and plasma oxidation on SiO_2 or diamond-like carbon (DLC) substrate. The highly-selective adsorption of 127-nm-sided triangular DNA origami structures were achieved due to the fact that the hydrophilic oxide surface attracts the negatively charged DNA while a hydrophobic

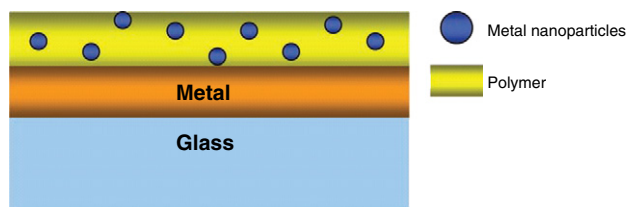


Fig. 27. Schematic illustration of the TCM system that consists of a glass substrate, a 25-nm gold film, and a polymer containing silver nanoparticles. Fig. reproduced from Ref. [331] with kind permission, © WILEY-VCH Verlag GmbH & Co. KGaA, Weinheim.

surface does not. This strategy was then used to produce 2-D arrays that consist of similar triangular DNA origami structures with corner-attached T8- or T30-conjugated 5 nm Au nanoparticles (Fig. 28(A)) [341]. A more elaborate strategy that creates ordered DNA origami arrays attached to predefined discrete Au islands on a Si substrate (Fig. 28(B)) [342] was also recently reported.

A conventional e-beam lithography (EBL) and lift-off process was used to generate the discrete Au island arrays. The chip was immersed and incubated in a solution containing thiolated DNA strands extended from both ends of DNA origami nanotubes. Very recently, Davis and colleagues [342] constructed DNA origami networks at even smaller scales to interconnect Au island arrays patterned from block copolymer etching. Instead of the standard EBL/lift-off process, a much denser array of Au nanoparticles (5 nm dia. and 62 nm center-to-center interspacing) was produced by O_2/Ar_2 plasma etching of a close-packed monolayer containing micelle encapsulated Au nanoparticles. The thiol-derivatized ssDNA subsequently reacted with and attached to the Au islands. This was followed by base-pairing with DNA origami structures to complete the patterning, see Fig. 28(C). The benefits of this work are threefold. First, the binding sites and origami length scale are one order of magnitude smaller (5 nm vs. 60 nm) as compared to Ref. [341], enabling nanoscale surface patterning and fabrication at even higher density. Second, steric hindering effectively suppresses the occurrence of multiply binding events, leading to higher yield as compared to Ref. [341]. Third, block-copolymer self-assembly (BCS) holds great promise in becoming a major player in nanoelectronics fabrication [343]. Thus, the marriage of DNA nanostructures and BCS is also of practical significance.

Although DNA possesses unique molecular recognition and self-assembly properties, its use in nanoelectronic interconnections and photonic enhancement necessitates that it be metallized for electrically conductive nanowires or plasmonic waveguides. To address these challenges, intensive efforts are underway to explore precisely controlled nanoscale metal deposition. Braun and coworkers [344] described a two-step approach for construction of a 12 μm long, 100 nm diameter Ag nanowire bridge between two micropatterned Au electrodes. First, λ -DNA was hybridized to ssDNA attached to the both sides of the electrode to form a DNA bridge. Ag^+ was then formed on the bridge via Na^+/Ag^+ ion exchange and reduced to Ag seeds in a basic hydroquinone solution followed by full growth in a Ag^+ containing acidic hydroquinone solution. Sequence-specific selective metallization was also studied with several systems.

In an approach called sequence-specific molecular lithography [345], nucleoprotein filaments (formed via polymerization of protein RecA on a ssDNA molecule and bound to aldehyde-derivatized dsDNA substrate) act as a mask to prevent Ag metallization from occurring at these specific locations. Instead of masking, information can also be encoded into the DNA scaffold to direct sequence-specific metal growth. For example, the organic component glutaraldehyde derivatized into the DNA scaffold molecule guides localized sequence-specific metal growth because it is an effective reducing agent [346]. Due to this reduction, a catalytic Ag cluster chain is formed along the DNA followed by electroless Au deposition to complete the fabrication of Au nanowires that measure a few micrometer long and ~ 50 nm in diameter. Because of differential binding affinities of nucleobases and Ag ions in an order of $\text{C} > \text{G} > \text{A} \geq \text{T}$ from strong to weak, Ag doublets and triplets could also be programmed and formed along single-strand DNA oligonucleotide scaffolds using [347].

In addition to 1-D metal structures, Kiehl, Seeman and co-workers [348] constructed 2D Au nanocomponent arrays by the in-situ hybridization of DNA-Au conjugates to predefined 2-D DNA scaffolds on a mica substrate (Fig. 29(A)). Recently, Harb and coworkers [349] utilized electroless plating to achieve continuous Au coating on isolated T- and Y-shaped branched DNA origami seeded with Ag. The result indicates that the origami maintains their shapes and the diameters of coated tubes can be as small as 32 nm. Therefore, it is

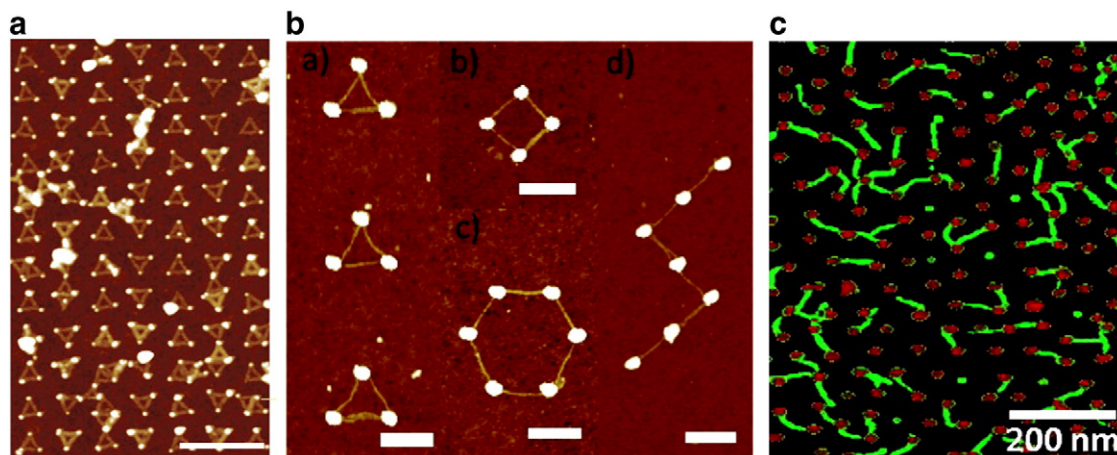


Fig. 28. Patterned DNA origami with Au nanoparticles or islands on substrates: (A) AFM image of DNA origami and T8-coated Au nanoparticle (bright dots) array formed on the sites of 100-nm-sided equilateral triangles defined with EBL on SiO₂. Scale bar, 500 nm. Fig. reproduced from Ref. [341] with kind permission, © Nature Publishing Group. (B) AFM image of DNA origami nanotubes connected to discrete Au islands defined with EBL/lift-off process in the shapes of (a) triangle, (b) hexagon, (c) square and (d) “z” on SiO₂. All scale bars, 300 nm. Fig. reproduced from Ref. [342] with kind permission, © American Chemical Society. (C) Tapping-mode AFM images of DNA origami attached to block copolymer patterned Au nanoparticles on the complementary ssDNA surface. Fig. reproduced from Ref. [343] with kind permission, © American Chemical Society.

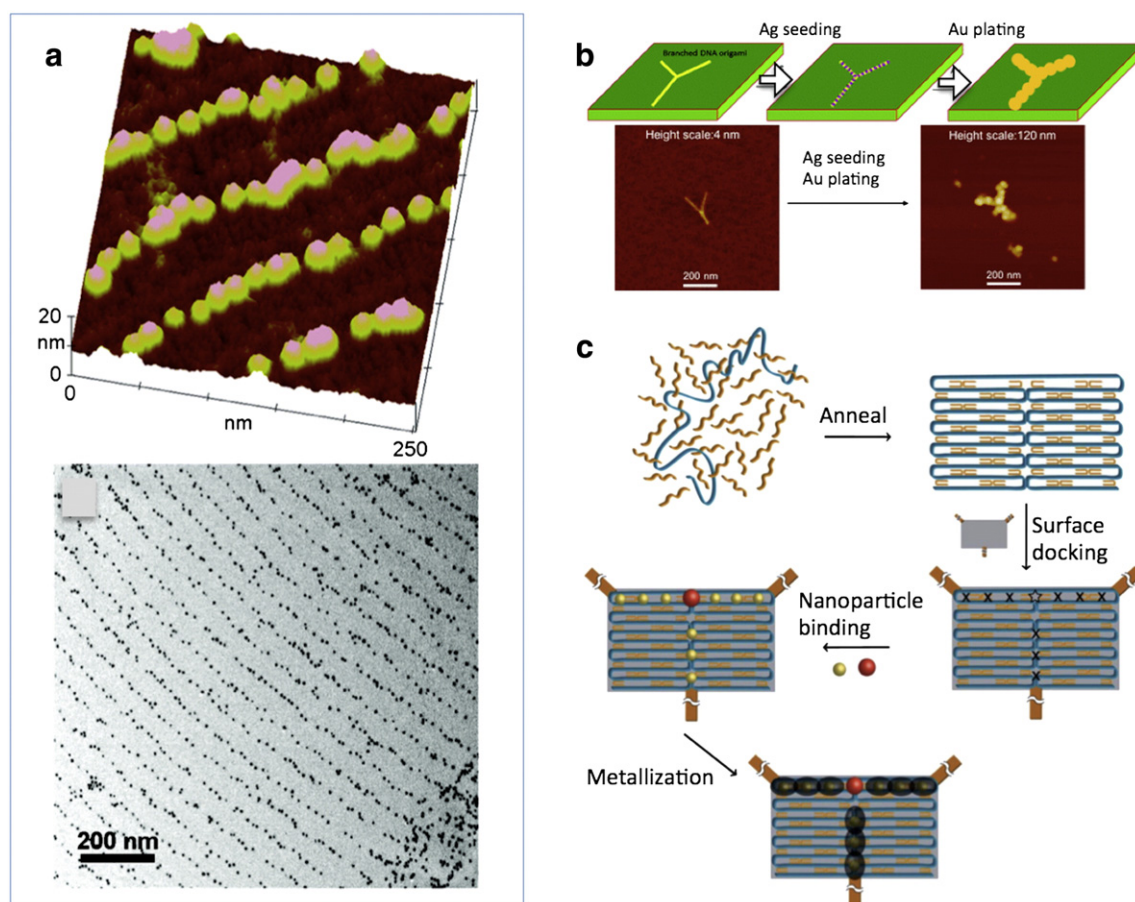


Fig. 29. Metallized DNA structures: (a) Self-assembled high-density 2-D Au array via hybridization of DNA-Au to a preassembled 2-D DNA scaffold. Top panel: AFM image of an assembled array of the DNA-Au nanocomponents, DNA marker rows, and DNA scaffolding. Bottom panel: TEM image of the 2-D nanocomponent array with Au particles of approximately 6.2 nm. Fig. reproduced from Ref. [349] with kind permission, © American Chemical Society. (b) Au metallization process of Y-shaped branched origami by seeding with Ag and subsequent electroless Au deposition. Bottom panel shows AFM images of DNA origami before and after metallization. Scale bar: 500 nm. Fig. reproduced from Ref. [350] with kind permission, © American Chemical Society. (c) A proposed schema for high-precision selective metallization using DNA origami. The process consists of forming DNA origami by annealing ssDNA scaffold strand (blue) with ssDNA staple strands (orange), positioning the DNA origami into desired binding sites (star and XOs) in a specific orientation on an electrode (brown)-containing surface, attaching nanoparticles (red and yellow) to their complementary sites on the origami, and depositing metal on the metallic nanoparticles (yellow) to produce nanowires that connects the electrodes, but the central island (red) is not connected. Fig. reproduced from Ref. [351] with kind permission, © The Royal Society of Chemistry.

possible to self-assemble more complex NP patterns using addressable DNA nanogrids. This would allow for the creation of NP constructs that may lead to applications in electronic, optic and photonic materials. These selective processes allow for metallic features to be embedded in the DNA scaffold maintaining its biological and recognition functionalities simultaneously. However, the metal coating process usually metalizes the whole origami and fails to demonstrate the potentially great capability of origami that promises structural selectivities (such as single strand metallization) Fig. 29(B). A brave idea was recently proposed to construct more

precisely controlled localized metallization within DNA origami, see Fig. 29(C) [350].

4. Conclusion and perspective on future advances in nanofabrication and technological implications

The last decade has seen amazing advances in nanofabrication techniques (both top–down and bottom–up) that have revolutionized developments of advanced nanomaterials with unprecedented

Table 1

A summary of the merits and demerits of top–down and bottom–up nanofabrication techniques.

Top–down method	Merits	Demerits	General remarks
Optical lithography	Long-standing, established micro/nanofabrication tool especially for chip production, sufficient level of resolution at high throughputs	Tradeoff between resist process sensitivity and resolution, involves state-of-the-art expensive clean room based complex operations	The 193 nm lithography infrastructure already reached a certain level of maturity and sophistication, and the approach could be extended to extreme ultraviolet (EUV) sources to shrink the dimension. Also, future developments need to address the growing cost of a mask set.
E-beam lithography	Popular in research environments, an extremely accurate method and effective nanofabrication tool for <20 nm nanostructure fabrication with desired shape	Expensive, low throughput and a slow process (serial writing process), difficult for <5 nm nanofabrication	E-beam lithography beats the diffraction limit of light, capable of making periodic nanostructure features. In the future, multiple electron beam approaches to lithography would be required to increase the throughput and degree of parallelism.
Soft & nanoimprint lithography	Pattern transfer based simple, effective nanofabrication tool for fabricating ultra-small features (<10 nm)	Difficult for large-scale production of densely packed nanostructures, also dependent on other lithography techniques to generate the template, and usually not cost-effective	Self-assembled nanostructures could be a viable solution to the problem of complex and costly template generation, and for templates of periodic patterns of <10 nm.
Block co-polymer lithography	A high-throughput, low-cost method, suitable for large scale densely packed nanostructures, diverse shapes of nanostructures, including spheres, cylinders, lamellae possible to fabricate including parallel assembly	Difficult to make self-assembled nanopatterns with variable periodicity required for many functional applications, usually high defect densities in block copolymer self-assembled patterns	Use of triblock copolymers is promising to generate more exotic nanopattern geometries. Also, functionalization of parts of the block copolymer could be done to achieve hierarchy of nanopatterning in a single step nanofabrication process.
Scanning probe lithography	High resolution chemical, molecular and mechanical nanopatterning capabilities, accurately controlled nanopatterns in resists for transfer to silicon, ability to manipulate big molecules and individual atoms	Limited for high throughput applications and manufacturing, an expensive process, particularly in the case of ultra-high-vacuum based scanning probe lithography	Scanning probe lithography can be leveraged for advanced bionanofabrication that involves fabrication of highly periodic biomolecular nanostructures.
Bottom–up method	Merits	Demerits	General remarks
Atomic layer deposition	Allows digital thickness control to the atomic level precision by depositing one atomic layer at a time, pin-hole free nanostructured films over large areas, good reproducibility and adhesion due to the formation of chemical bonds at the first atomic layer	Usually a slow process, also an expensive method due to the involvement of vacuum components, difficult to deposit certain metals, multicomponent oxides, certain technologically important semiconductors (Si, Ge etc.) in a cost-effective way	Although a slow process, it is not detrimental for the fabrication of future generation ultra-thin ICs. The stringent requirements for the metal barriers (pure; dense; conductive; conformal; thin) that are employed in modern Cu-based chips can be fulfilled by atomic layer deposition.
Sol gel nanofabrication	A low-cost chemical synthesis process based method, fabrication of a wide variety of nanomaterials including multicomponent materials (glass, ceramic, film, fiber, composite materials),	Not easily scalable, usually difficult to control synthesis and the subsequent drying steps	A versatile nanofabrication method that can be made scalable with further advances in the synthesis steps.
Molecular self assembly	Allows self assembly of deep molecular nanopatterns of width less than 20 nm and with the large pattern stretches, generates atomically precise nanosystems	Difficult to design and fabricate nanosystems unlike mechanically directed assembly	Molecular self assembly of multiple materials may be a useful approach in developing multifunctional nanosystems and devices.
Physical and chemical vapor-phase deposition	Versatile nanofabrication tools for fabrication of nanomaterials including complex multicomponent nanosystems (e.g. nanocomposites), controlled simultaneous deposition of several materials including metal, ceramics, semiconductors, insulators and polymers, high purity nanofilms, a scalable process, possibility to deposit porous nanofilms	Not cost-effective because of the expensive vacuum components, high-temperature process and toxic and corrosive gases particularly in the case of chemical vapor deposition	It provides unique opportunity of nanofabrication of highly complex nanostructures made of distinctly different materials with different properties that are not possible to accomplish using most of the other nanofabrication techniques. New advances in chemical vapor deposition such as 'initiated chemical vapor deposition' (i-CVD) provide unprecedented opportunities of depositing polymers without reduction in the molecular weights.
DNA-scaffolding	Allows high-precision assembling of nanoscale components into programmable arrangements with much smaller dimensions (less than 10 nm in half-pitch).	Many issues need to explore, such as novel unit and integration processes, compatibility with CMOS fabrication, line edge roughness, throughput and cost.	Very early stage. Ultimate success depends on the willingness of the semiconductor industry in terms of need, infrastructural capital investment, yield and manufacturing cost.

functional properties. Extension of existing nanofabrication techniques will facilitate rapid development of microelectronic circuits with nanometer scale features. Future research needs to be directed towards the development of novel techniques and materials required for the generation of structures with dimensions below ~10 nm. Outside the field of microelectronics, new nanofabrication techniques that take advantage of the combination of top-down and bottom-up approaches must be developed for new products and technologies applied in different research areas ranging from biology and medicine to materials science and electronics. Top-down methods that have been covered in this review include lithography-based techniques. While optical lithography remains a popular technique in the microelectronics/nanoelectronics arena, and the feature size below 50 nm is achievable using the current infrastructure, the technique remains very expensive. Future research on nanomaterials fabrication will depend on the less-expensive processes in order to produce low-cost nanomaterials and devices. In this regard, one viable approach for optical lithography processes could be less-dependencies on the state-of-the-art very expensive clean room operations. Electron beam lithography is a powerful tool to generate much smaller structures (~10 nm) with the possibility of highly reproducible nanostructures with desired shapes. We already have seen unique nanomaterials and devices fabricated by electron beam lithography. But, the low throughput remains an important challenge to be overcome. A combination of optical and electron beam lithography has already been thought for a viable approach towards this end, which could be leveraged to fabricate very exotic nanostructures and devices in the future with unprecedented precision and functional properties. The current state-of-the-art scanning probe lithography allows parallel fabrication of structures at the molecular scale. The development in this area has been fascinating. Molecular electronics or functional devices have been made possible to realize by the applications of scanning probe lithography methods. We envision that the scanning probe lithography based methods will continue to evolve over the next decade that will address the low-throughput issues. We also envision that nanoimprint-based lithography will continue to develop into a more practical method for large-scale fabrication of devices particularly in the areas of photovoltaics and energy materials arenas.

The bottom-up methods described in this review have shown tremendous promise in realizing very complex nanostructures that are difficult to achieve by the usual top-down processes. Complex technologies in the future will need combination of nanoscale materials with competing properties in a single system for viable material solutions to some of the most difficult technological challenges. Bottom-up nanofabrication techniques such as self-assembly, vapor-deposition or sol-gel processes provide unique opportunities in combinatorial nanomaterials fabrication. A continuation of the use of these techniques is anticipated in the future for the fabrication of multi-component nanomaterial systems such as nanocomposites.

We have summarized various nanofabrication techniques described in this review in Tables 1 and 2. In Table 1, we have described the techniques with respect to advantages and disadvantages of each technique. Table 2 shows the comparison of the various parameters such as resolution or size, complexity/defectivity and material limitation for the various nanofabrication methods.

The exciting progress to date suggests that the field of nanofabrication will not only continue to advance its current frontiers and respond to the needs of the electronics industry but is also uniquely positioned to take on new challenges in the development of novel biomedical and energy-related technologies. In biomedicine, for example, developments in nanofabrication tools will allow production of ever smaller and more sensitive diagnostic and therapeutic probes to accommodate an enormous number of biological structures and functions. Particularly, in the future, an exciting possibility could be combining scanning probe lithography with bionanofabrication techniques to realize unique biomacromolecular structures and devices with unprecedented functional properties that could transform the areas of bionanotechnology-based advanced medicine for future therapy and drug-delivery etc. The ability to construct sophisticated surfaces with functional chemicals and in controlled chemical environments will enable understanding and mimicking of biological systems and processes. Synthetic organic chemists will continue to focus on methodologies to construct the complex molecules that cater to pharmacological targets inspired by natural products. Over the next two decades, the field is anticipated to focus on organic supramolecular chemistry to create soft functional nanostructures, including the exploration of their physical properties and use as components of materials and macroscopic devices.

The major motivating factor for pushing towards further advances in DNA nanoelectronics fabrication stems apparently from the fact that DNA offers a much smaller one dimension (less than 10 nm in half-pitch) that is out of the paradigm of the capability of the current semiconductor industry. However, nanoelectronics fabrication involves many sophisticated unit processes and requirements. For these to be inserted in certain fabrication steps, the biologically-based DNA nanotechnology must not only be compatible with CMOS process but also meet stringent requirements such as line edge roughness and throughput. In spite of the inspirational and rapid pace in developments toward this direction, this emerging area remains in its early infancy. Many important issues, ranging from fundamental unit processes to overall integration, need to be addressed. For example, future challenges include arbitrary geometries, multilevel patterning at molecular resolution, molecularly accurate device localization, more material selections with dielectricity etc. Even if this technology becomes mature, the determinant of its adoption ultimately relies on the willingness of the semiconductor industry in terms of need, infrastructural capital investment, yield and manufacturing cost.

New nanostructured devices are emerging as sensitive bioanalysis platforms based on unique optical and electrical properties due to nanofabrication. For example, dual optical switches for DNA sequence

Table 2

A comparison of the materials parameters for the various nanofabrication techniques.

Methods	Resolution/size	Nanofabrication complexity	Nanostructural defectivity	Materials range	Layering possibility
Optical lithography	~50 nm	High	Low	Inorganic and organic	No
E-beam lithography	~10 nm	High	Extremely low	Mostly inorganic	No
Nanoimprint lithography	~5–10 nm	Higher for roll-to-roll processes	Low	Inorganic and organic	Difficult
Scanning probe lithography	<5 nm	High	Extremely low	Mostly organic	No
Block co-polymer lithography	~10 nm	Low	Low	Inorganic and organic	No
Atomic layer deposition	<5 nm	High	Extremely Low	Mostly inorganic	Yes
Sol-gel	~50 nm	High	High	Mostly inorganic	No
Molecular, layer-by-layer and directed self assembly	<5 nm	Low	Low	Inorganic and organic	Yes
Physical and chemical vapor phase deposition	<5 nm	High	Low–moderately high	Inorganic, organic, ceramic, insulator, semiconductor	Yes
DNA scaffolding	<10 nm	High	Low	Inorganic and organic	Yes

analysis based on fluorescence quenching and simultaneous Raman scattering of gold nanoparticle aggregates, Raman “hot spots” within synthesized dimers of silver cubes or spheres leading to enhanced sensitivity by factors of 20 million and bioelectrical “noses” based on human olfactory receptor-coated SWNT-FET (field effect transistor) that afford detection of odorant molecules with single carbon mismatches have already emerged. In addition, nanofabrication has allowed understanding and manipulation of a large number of complex processes in bio-targeting, ranging from drug delivery, bone-inspired biomedical scaffolds to eye-tissue regeneration, to self-organization and responsive behavior. As new materials and nanofabrication tools become available, biomedicine will increasingly depend upon more and more methods of nanofabrication enabling the emergence of new techniques. In summary, nanofabrication will continue to grow and convert nanosciences into an indispensable technology of the future.

Acknowledgements

The authors from Notre Dame (AB and TW) acknowledge the financial support provided by the center for Nano Science and Technology (NDnano). The editorial assistance of Dr. Marinelle Ringer is appreciated.

References

- Ariga K, Hill JP, Lee MV, Vinu A, Charvet R, Acharya S. *Sci Technol Adv Mater* 2008;9:014109.
- Sakakibara K, Hill JP, Ariga K. *Small* 2008;7:1288.
- Ariga K, Lee MV, Mori T, Yu Xiao-Yan, Hill JP. *Adv Colloid Interface Sci* 2008;154:20.
- Ariga K, Li M, Richards GJ, Hill JP. *J Nanosci Nanotechnol* 2008;11:1.
- Acharya S, Hill JP, Ariga K. *Adv Mater* 2008;21:2959.
- Ariga K, Hill JP, Ji Q. *Phys Chem Chem Phys* 2008;9:2319.
- Gates BD, Qiaobing Xu, Stewart M, Ryan D, Willson CG, Whitesides GM. *Chem Rev* 2005;105:1171.
- Linjie Li, Rafael RG, Gershgoren E, Hwang H, Fourkas JT. *Science* 2009;324:910.
- Schmid GM, et al. *J Vac Sci Technol B* 2009;27:573.
- Ginger DS, Zhang H, Mirkin CA. *Angew Chem Int Ed* 2004;43:30.
- Maily D. *Eur Phys J Special Topics* 2009;172:333.
- Ando Y, Miyake K, Mizuno A, Korenaga A, Nakano M, Mano H. *Nanotechnology* 2009;21:095304.
- Unconventional Nanopatterning Techniques and Applications, Lee Hong H. In: Rogers John A, editor. Wiley978-0-470-09957-5; 2008.
- Kraemer S, Fuierer RR, Gorman CB. *Chem Rev* 2009;103:4367.
- Marrinan CRK, Tennant DM. *J Vac Sci Technol A* 2009;21:S207.
- Yaman M, Khudiyev T, Ozgur E, Kanik M, Aktas O, Ozgur EO, Deniz H, Korkut E, Bayindir M. *Nat Mater* 2009;10:494.
- Liddle JA, Gallatin GM. *Nano Scale* 2009;3:2679.
- Lee KB, Lim JH, Mirkin CA. *J Am Chem Soc* 2003;125:5588.
- Smith JC, Lee KB, Wang Q, Finn MG, Johnson JE, Mirkin CA. *Nano Lett* 2003;3:883.
- Biswas A, Eilers H, Hidden F, Aktas OC, Kiran CVS. *Appl Phys Lett* 2006;88:013103.
- Schäffer E, Thurn-Albrecht T, Russell TP, et al. *Nature* 2000;403:874.
- Hoelen W, Duesberg GS, Graham AP, Kreupl F, Liebau M, Pamler W, Seidel R, Unger E. *Microelectron Eng* 2006;83:619.
- Handbook of Microlithography. Micromachining and Microfabrication. In: Rai chowdhury P, editor. Microlithography, Vol. 1. Bellingham, WA: SPIE; 1997.
- Shingi H, Masato S, Eiichi T, Hideki M. *J Vac Sci & Tech B: Microelectronics and Nanometer Structures* 2003;21:2937.
- Born M, Wolf E. *Principles of Optics* (Cambridge University Press), ISBN 0521642221.
- Maria J, Malyarchuk V, White J, Rogers JA. *J Vac Sci Technol B* 2006;24:828.
- Do J, Cui Z, Yuan X, Guo Y. *Microelectron Eng* 2002;61–62:265.
- Ito T, Okazaki S. *Nature* 2000;406:1027.
- French RH, Tran HV. *Annu Rev Mater Res* 2009;39:93.
- Moon JH, Yang Seung-Man, Pine DJ, Chang Won-Seok. *Appl Phys Lett* 2004;85:4184.
- Smayling MC, Axelrad V. 32 nm and below Logic Patterning using Optimized Illumination and Double Patterning, Optical Microlithography XXII. In: Levinson Harry J, Dusa Mircea V, editors. Proceedings of the SPIE 2009;7274:72740K.
- Wu B, Kumar A. *Extreme Ultraviolet Lithography*. 1 edition. McGraw-Hill Professional; 2009. ISBN-13: 978-0071549189.
- Tae-Seung E, Sarohan P, Jun-Taek PARK, Chang-Moon L, Sunyoung K, Yoon-Suk H, Hyeongsoo K, Byoung-Ho N, Chang-Reol K, Seung-Chan M, Noh-Jung K, Sungki P. Comparative Study of DRAM Cell Patterning between ArF Immersion and EUV Lithography. Proceedings of SPIE, the International Society for Optical Engineering 0277-786X, Vol. 7271 (2)978-0-8194-7524-4; 2009.
- Li SP, Peyrade D, Natali M, Lebib A, Chen Y, Ebels U, Buda LD, Ounadjela K. *Phys Rev Lett* 2001;86:1102 and the references therein.
- Broers AN. *Philosophical Transactions of the Royal Society of London Series – Mathematical. Phys Eng Sci* 1995;353:291.
- Berger SD, Gibson JM. *Appl Phys Lett* 1990;57:153.
- Tseng AA, Chen K, Chen CD, Ma KJ. *IEEE Trans Elec Pack Man* 2003;26:1523.
- Driskill-Smith AAG, Katine JA, Druist DP, Lee KY, Tiberio RC, Chiu A. *Microelectron Eng* 2004;73–74:547.
- Br’etagnon F, Sirghi L, Mornet S, Sasaki T, Gilliland D, Colpo P, Rossi F. *Nanotechnology* 2008;19:125306.
- Burek MJ, Greer JR. *Nano Lett* 2010;10:69.
- Whitesides GM, Stroock AD. *Physics Today* 2001;54:42.
- Kim YS, Lee NY, Lim JR, Lee MJ, Park S. *Chem Mater* 2005;17:5867.
- Lee KJ, Jin J, Bae Byeong-Soo, Magnusson R. *Opt Lett* 2009;34:2510.
- Schmid H, Michel B. *Macromolecules* 2000;33:3042.
- Odum TW, Lowe JC, Wolfe DB, Paul KE, Whitesides GW. *Langmuir* 2002;18:5314.
- Lee T-W, Mitrofanov O, Hsu JWP. *Adv Funct Mater* 2005;15:1683.
- Tang MD, Golden AP, Tien J. *J Am Chem Soc* 2003;125:12988.
- Rogers JA, Nuzzo RG. *Materials Today* 2005;8:50.
- Lee D-H, Park K-H, Hong L-Y, Kim D-P. *Sens Actuators A* 2007;135:895.
- Viswanathan M, Yelizaveta B, Odum TW. *J Chem Educ* 2007;84:1795.
- Pokroy B, Epstein AK, Persson-Gulda MCM, Aizenberg J. *Adv Mater* 2009;21:463.
- Betancourt T, Brannon-Peppas L. *Int J Nanomedicine* 2006;1:483.
- Lia SP, Natali M, Lebib A, P’epin A, Chen Y, Xu YB. *J Magn Magn Mater* 2002;241:447.
- Michel B, Bernard A, Bietsch A, Delamarche E, Geissler E, Juncker D, Kind H, Renaud JP, Rothuizen H, Schmid H, Schmidt-Winkel P, Stutz R, Wolf H. *IBM J Res & Dev* 2001;45:697.
- Kim YS, Lee HH, Hammond PT. *Nanotechnology* 2003;14:1140.
- Guo LJ. *J Phys D: Appl Phys* 2004;37:R123 and the references there in.
- Chou SY, Krauss PR, Renstrom PJ. *Science* 1996;272:85.
- Hsu KH, Schultz PL, Ferreira PM, Fang NX. *Nano Lett* 2007;7:446.
- GuoYong X, Zhang J, Zhang YY, Zhang YY, Zhu T, Liu ZF. *Sci China Ser E-Tech Sci* 2009;52:1181.
- Bergmair I, et al. *Nanotechnology* 2011;22:325301.
- Gao H, Tan H, Zhang W, Morton K, Chou SY. *Nano Lett* 2006;6:2438.
- Viheriälä J, Niemi T, Kontio J, Rytönen T, Pessa M. *Electron Lett* 2007;47:150.
- Kostovski G, White DJ, Mitchell A, Austin M, Stoddart PR. *Biosens Bioelectron* 2009;24:1531.
- Kumar G, Tang H, Schroers J. *Nature* 2009;457:868.
- Hiroshima H, Komuro M. *Jpn J Appl Phys* 2007;46:6391.
- Landis S, et al. *Nanotechnology* 2006;17:2701.
- Bailey TC, et al. *Microelectron Eng* 2002;61:461.
- Dauksher WJ, et al. *J Vac Sci Technol B* 2002;20:2857.
- Bailey T, Choi BJ, Colburn M, Meissl M, Shaya S, Ekerdt JG, Sreenivasan SV, Willson CG. *J Vac Sci Technol B* 2000;18:3572.
- Resnick DJ, et al. *J Vac Sci Technol B* 2003;21:2624.
- Taniguchi J, Tokano Y, Miyamoto I, Komuro M, Hiroshima H. *Nanotechnology* 2002;13:592.
- Beck M, Graczyk M, Maximov I, Sarwe EL, Ling TGI, Keil M, Montelius L. *Microelectron Eng* 2002;61:441.
- Khang DY, Kang H, Kim T, Lee HH. *Nano Lett* 2004;4:633.
- Khang DY, Lee HH. *Langmuir* 2004;20:2445.
- Jung GY, Ganapathiappan S, Li X, Ohlberg DAA, Olynick DL, Chen Y, Tong WM, Williams RS. *Appl Phys A: Mater Sci Process* 2004;78:1169.
- Khang DY, Lee HH. *Appl Phys Lett* 2000;76:870.
- Hirai Y, Fujiwara M, Okuno T, Tanaka Y, Endo M, Irie S, Nakagawa K, Sasago M. *J Vac Sci Technol B* 2001;19:2811.
- Khang DY, Yoon H, Lee HH. *Adv Mater* 2001;13:749.
- Schiff H, Heyderman LJ, Maur MAD, Gobrecht J. *Nanotechnology* 2001;12:173.
- Heyderman LJ, Schiff H, David C, Gobrecht J, Schweizer T. *Microelectron Eng* 2000;54:229.
- Scheer HC, Schulz H. *Microelectron Eng* 2001;56:311.
- Pfeiffer K, Fink A, Gruetzner G, Bleidiessel G, Schulz H, Scheer H. *Microelectron Eng* 2001;57:381.
- Montelius L, Heidari B, Graczyk M, Maximov I, Sarwe EL, Ling TGI. *Microelectron Eng* 2000;53:521.
- Cheng X, Guo LJ. *Microelectron Eng* 2004;71:288.
- Hirai Y, Kikuta H, Sanou T. *J Vac Sci Technol B* 2003;21:2777.
- Kunz R, Rothschild RM, Yeung MS. *J Vac Sci Technol B* 2003;21:78.
- Goodberlet JG, Kavak H. *Appl Phys Lett* 2002;81:1315.
- Cao H, Yu ZN, Wang J, Tegenfeldt JO, Austin RH, Chen E, Wu W, Chou SY. *Appl Phys Lett* 2002;81:174.
- Cao H, Tegenfeldt JO, Austin RH, Chou SY. *Appl Phys Lett* 2002;81:3058.
- Guo LJ, Cheng X, Chou CF. *Nano Lett* 2004;4:69.
- Chao YJ, Guo LJ. *Appl Phys Lett* 2004;83:1527.
- Chen Y, Douglas AA, Li OX, Duncan R, Stewart R, Williams S, Jeppesen JO, Nielsen KA, Stoddart JF, Olynick DL, Anderson E. *Appl Phys Lett* 2003;82:1610.
- Yang R, Lu Bing-Rui, Wan J, Xie Shen-Qi, Chen Y, Huq E, Qu Xin-Ping, Liu R. *Microelectron Eng* 2009;86:1379.
- Dumond JJ, Low HY, Rodriguez I. *Nanotechnology* 2006;17:1975.
- Abad E, Merino S, Retolaza A, Juarros A. *Microelectron Eng* 2008;85:818.
- Li W, Tegenfeldt JO, Chen L, Austin RH, Chou SY, Kohl PA, Krotine J, Sturm JC. *Nanotechnology* 2003;14:578.
- Levene MJ, Korlach J, Turner SW, Foquet M, Craighead HG, Webb WW. *Science* 2003;299:682.

- Tegenfeldt JO, Bakajin O, Chou C-F, Chan S, Austin RH, Chan E, Duke T, Cox EC. *Phys Rev Lett* 2003;86:1378.
- [86] Kreindl G, Glinsner T, Miller R. *Nature Photonics* 2010;4:27.
- [87] Liang X, Chou SY. *Nano Lett* 2008;8:1472.
- [88] Hoff JD, Cheng LJ, Meyhofer E, Guo LJ, Hunt AJ. *Nano Lett* 2004;4:853.
- [89] Wang Y, Goh SH, Bi X, Yang KL. *J Colloid Interface Sci* 2009;333:188.
- [90] Liang X, Morton KJ, Austin RH, Chou SY. *Nano Lett* 2007;7:3774.
- [91] Boltasseva AJ. *Opt A: Pure Appl Opt* 2009;11:114001.
- [92] Pedersen RH, Boltasseva A, Johansen DM, Nielsen T, Jørgensen KB, Leosson K, Erland J, Kristensen A. *Microelectron Eng* 2007;84:895.
- [93] Yang JKW, Jung YS, Chang Jae-Byum, Mickiewicz RA, Alexander-Katz A, Ross CA, Berggren KK. *Nat Nanotechnol* 2010;5:256.
- [94] Poelma JE, Hawker CJ. *News and views. Nat Nanotechnol* 2010;5:243.
- [95] Hamley IW. *Nanotechnology* 2003;14:R39.
- [96] Bang J, Jeong U, Ryu DY, Russell TP, Hawker CJ. *Adv Mater* 2009;21:1.
- [97] Stoykovich MP, et al. *Science* 2005;308:1442.
- [98] Bitá I, et al. *Science* 2008;321:939.
- [99] Cheng JY, Rettner CT, Sanders DP, Kim HC, Hinsberg WD. *Adv Mater* 2008;20:3155.
- [100] Ruiz R, et al. *Science* 2008;321:936.
- [101] Park S, et al. *Science* 2009;323:1030.
- [102] Kim S, et al. *Nature* 2003;424:411.
- [103] Wilmes GM, Durkee DA, Balsara NP, Liddle JA. *Macromolecules* 2006;39:2435.
- [104] Segalman RA, Hexemer A, Kramer EJ. *Phys Rev Lett* 2003;91:192101.
- [105] Segalman RA, Yokoyama H, Kramer EJ. *Adv Mater* 2001;13:1152.
- [106] Stoykovich MP, et al. *ACS Nano* 2007;1:168.
- [107] Sundrani D, Darling SB, Sibener SJ. *Nano Lett* 2004;4:273.
- [108] Black CT, Bezenecenet O. *IEEE Trans Nanotechnol* 2004;3:412.
- [109] Cheng JY, Mayes AM, Ross CA. *Nature Mater* 2004;3:823.
- [110] Park SM, Craig GSW, La YH, Solak HH, Nealey PF. *Macromolecules* 2007;40:5084.
- [111] Tang CB, Lennon EM, Fredrickson GH, Kramer EJ, Hawker CJ. *Science* 2008;322:429.
- [112] Bang J, et al. *J Am Chem Soc* 2008;128:7622.
- [113] Hawker CJ, Russell TP. *MRS Bulletin* 2005;30:952.
- [114] Kim S-J, Maeng WJ, Lee SK, Park DH, Bang SH, Kim H, Sohn B-H. *J Vac Sci Technol B: Microelectron Nanometer Struct* 2008;26:189.
- [115] Cheng JY, Ross CA, Smith HI, Thomas EL. *Adv Mater* 2006;18:2505.
- [116] Glass R, M'oller M, Spatz JP. *Nanotechnology* 2003;14:1153.
- [117] Lee W-K, Sheehan PE. *Scanning* 2008;30:172.
- [118] Hong S, Mirkin CA. *Science* 2000;288:1808.
- [119] Ryu KS, Wang X, Shaikh K, Bullen D, Goluch E, Zou J, Liu C, Mirkin CA. *Appl Phys Lett* 2004;85:136.
- [120] Frolov VD, Konov VI, Pimenov SM, Kosheleva SV. *J Phys: Conf Ser* 2011;291:012035.
- [121] Smith JC, Lee K-B, Wang Q, Finn MG, Johnson JE, Mrksich M, Mirkin CA. *Nano Lett* 2003;3:883.
- [122] Lee K-B, Kim E-Y, Mirkin CA, Wolinsky SM. *Nano Lett* 2004;4:1869.
- [123] Nam J-M, Han SW, Lee K-B, Liu X, Ratner MA, Mirkin CA. *Angew Chem Int Ed* 2004;43:1246.
- [124] Zhang H, Mirkin CA. *Chem Mater* 2004;16:1480.
- [125] Zhang H, Chung S-W, Mirkin CA. *Nano Lett* 2003;3:43.
- [126] Rozhok S, Piner R, Mirkin CA. *J Phys Chem B* 2003;107:751.
- [127] Schwartz PV. *Langmuir* 2001;17:5971.
- [128] Schwartz PV. *Langmuir* 2002;18:4041.
- [129] Jang J, Schatz GC, Ratner MA. *Phys Rev Lett* 2004;92:08550401.
- [130] Jang J, Schatz GC, Ratner MA. *Phys Rev Lett* 2003;90:15610401.
- [131] Jang J, Hong S, Schatz GC, Ratner MA. *J Chem Phys* 2001;115:2721.
- [132] Liu J-F, Cruchon-Dupeyrat S, Garno JC, Frommer J, Liu G-Y. *Nano Lett* 2002;2:937.
- [133] Liu G-Y, Xu S, Qian Y. *Acc Chem Res* 2000;33:457.
- [134] Rolandi M, Suez I, Dai H, Fréchet JM. *Nano Lett* 2004;4:889.
- [135] Garno JC, Yang Y, Amro NA, Cruchon-Dupeyrat S, Chen S, Liu G-Y. *Nano Lett* 2003;3:389.
- [136] Porter Jr LA, Ribbe AE, Buriak JM. *Nano Lett* 2003;3:1043.
- [137] Bouzehouane K, Fusil S, Bibes M, Carrey J, Blon T, Du ML, Seneor P, Cros V, Vila L. *Nano Lett* 2003;3:1599.
- [138] Liu S, Maoz R, Schmid G, Sagiv J. *Nano Lett* 2002;2:1055.
- [139] Maoz R, Frydman E, Cohen SR, Sagiv J. *Adv Mater* 2000;12:725.
- [140] Sun S, Leggett GJ. *Nano Lett* 2002;2:21223.
- [141] Sun S, Chong KSL, Leggett GJ. *J Am Chem Soc* 2002;124:2414.
- [142] Sun S, Leggett GJ. *Nano Lett* 2004;4:1381.
- [143] Salaita K, Wang Y, Mirkin CA. *Nat Nanotechnol* 2007;2:145.
- [144] Eigler DM, Schweizer EK. *Nature* 1990;344:524.
- [145] Crommie MF, Lutz CP, Eigler DM. *Science* 1993;262:218.
- [146] Wu CDa, Fang Te-H, Lin J-F. *Langmuir* 2010;26:3237.
- [147] Jaschke M, Butt HJ. *Langmuir* 1995;11:1061.
- [148] Noy A, Miller AE, Klare JE, Weeks BL, Woods BW, DeYoreo JJ. *Nano Lett* 2002;2:109.
- [149] Nafday OA, Vaughn MW, Weeks BL. *J Chem Phys* 2006;125:144703.
- [150] Cho Y, Ivanisevic A. *Langmuir* 2006;22:8670.
- [151] Suez I, Rolandi M, Backer SA, Scholl A, Doran A, Okawa D, Zettl A, Fréchet JM. *Adv Mater* 2007;19:3570.
- [152] Hoepfner S, Maoz R, Sagiv J. *Nano Lett* 2003;3:761.
- [153] Rosa LG, Jiang J, Lima OV, Xiao J, Utreras E, Dowben PA, Tan L. *Mater Lett* 2009;63:961.
- [154] Dagata JA, Schneir J, Harary HH, Evans CJ, Postek MT, Bennett J. *Appl Phys Lett* 1990;56:2001.
- [155] Dai H, Franklin N, Han J. *Appl Phys Lett* 1998;73:1508.
- [156] Lutwyche MI, Rothuizen HE, Stutz R, Widmer R, Binnig GK. *IBM J Res Dev* 2000;44:323.
- [157] Vettiger P, Binnig G. *Sci Am* 2003;1:47.
- [158] Bullen D, Chung S-W, Wang X, Zou J, Mirkin CA, Liu C. *Appl Phys Lett* 2004;84:789.
- [159] Zhang M, Bullen D, Chung S-W, Hong S, Ryu KS, Fan Z, Mirkin CA, Liu C. *Nanotechnology* 2002;13:212.
- [160] Lee W-K, Chen S, Chilkoti A, Zauscher S. *Small* 2007;3:249.
- [161] Park S, Wang WM, Bao Z. *Langmuir* 2010;26:6853.
- [162] Rolandi M, Suez I, Scholl A, Fréchet JM. *Angew Chem Int Ed* 2007;46:7477.
- [163] Werayut S, Pan L, Wang Y, Sun C, Bogy DB, Zhang X. *Nat Nanotechnol* 2008;3:733.
- [164] Leggett GJ. *Chem Soc Rev* 2006;35:1150.
- [165] Ducker R, Garcia A, Zhang J, Chen T, Zauscher S. *Soft Matter* 2008;4:1774.
- [166] Ducker RE, Leggett GJ. *J Am Chem Soc* 2006;128:392.
- [167] Novotny L, Stranick SJ. *Annu Rev Phys Chem* 2006;57:303.
- [168] Luo G, Xie G, Zhang Y, Zhang G, Zhang Y, Carlberg P, Zhu T, Liu Z. *Nanotechnology* 2006;17:3018.
- [169] Choi I, Kim Y, Yi J. *Ultramicroscopy* 2008;108:1205.
- [170] Suntola T, Antson J. *US Patent* 1977; 4 058 430.
- [171] George SM. *Chem Rev* 2010;110:111.
- [172] Knez M, Nielsch K, Niinistö L. *Adv Mater* 2007;19:3425.
- [173] Leskelä M, Kemell M, Kukli K, Pore V, Santala E, Ritala M, Lu J. *Mater Sci Eng C* 2007;27:1504.
- [174] Ritala M, Leskelä M. In: *Nalwa HS, editor. Handbook of Thin Film Materials*, 1. San Diego: Academic Press; 2002. p. 103.
- [175] Knez M, Kadri A, Wege C, Goesele U, Jeske H, Nielsch K. *Nano Lett* 2006;6:1172.
- [176] King DM, Johnson SI, Li J, Du X, Liang X, Weimer AW. *Nanotechnology* 2009;20:195401.
- [177] Kim H, Lee H-B-R, Maeng W-J. *Thin Solid Films* 2009;517:2563.
- [178] Huang J, Liu S, Wang Y, Ye Z. *Appl Surf Sci* 2008;254:5917.
- [179] Choi S-W, Park JY, Kim SS. *Nanotechnology* 2009;20:465603.
- [180] Park S, Jun J, Kim HW, Lee C. *Solid State Commun* 2009;149:315.
- [181] Paunesku T, Rajh T, Wiederrecht G, Maser J, Vogt S, Stojicevic N, Protic M, Lai B, Oryhon J, Thurnauer M, Woloschak G. *Nat Mater* 2003;2:343.
- [182] Paunesku T, Vogt S, Lai B, Maser J, Stojicevic N, Thurn KT, Osipo C, Liu H, Legnini D, Wang Z, Lee C, Woloschak GE. *Nano Lett* 2007;7:596.
- [183] Lopez T, Recillas S, Guevara P, Sotelo J, Alvarez M, Odriozola JA. *Acta Biomater* 2008;4:2037.
- [184] Kim H, Pippel E, Goesele U, Knez M. *Langmuir* 2009;25:13284.
- [185] Elam JW, Xiong G, Han CY, Wang HH, Birrell JP, Welp U, Hryn JN, Pellin MJ, Baumann TF, Poco JF, Satcher JH. *J Nanomater* 2006;22:1.
- [186] Martinson ABF, Elam JW, Hupp JT, Pellin MJ. *Nano Lett* 2007;7:2183.
- [187] Elam JW, Libera JA, Pellin MJ, Stair PC. *Appl Phys Lett* 2007;91:24.
- [188] Kemell M, Pore V, Tupala J, Ritala M, Leskelä M. *Chem Mater* 2007;19:1816.
- [189] Liao HC, Kuo PC, Lin CC, Chen SY. *J Vac Sci Technol B: Microelectron Nanometer Struct* 2006;24:2198.
- [190] Sander MS, Cote MJ, Gu W, Kile BM, Tripp CP. *Adv Mater* 2004;16:2052.
- [191] Daub M, Knez M, Goesele U, Nielsch K. *J Appl Phys* 2007;101:9.
- [192] Bachmann J, Jing J, Knez M, Barth S, Shen H, Mathur S, Goesele U, Nielsch K. *J Am Chem Soc* 2007;129:9554.
- [193] Yang CJ, Wang SM, Liang SW, Chang YH, Chen C, Shieh JM. *Appl Phys Lett* 2007;90:033104.
- [194] Tan LK, Chong ASM, Tang XSE, Gao H. *J Phys Chem C* 2007;111:4964.
- [195] Kim W-H, Park S-J, Son J-Y, Kim H. *Nanotechnology* 2008;19:045302.
- [196] Kucheyev SO, Biener J, Wang YM, Baumann TF, Wu KJ, van Buuren T, Hamza AV, Satcher Jr JH, Elam JW, Pellin MJ. *Appl Phys Lett* 2005;86:083108.
- [197] Elam JW, Libera JA, Pellin MJ, Zinovev AV, Greene JP, Nolen JA. *Appl Phys Lett* 2006;89:5.
- [198] Baumann TF, Biener J, Wang YM, Kucheyev SO, Nelson EJ, Satcher JH, Elam JW, Pellin MJ, Hamza AV. *Chem Mater* 2006;18:6106.
- [199] Biener J, Baumann TF, Wang YM, Nelson EJ, Kucheyev SO, Hamza AV, Kemell M, Ritala M, Leskelä M. *Nanotechnology* 2007;18:5.
- [200] Guarini KW, Black CT, Zhang Y, Kim H, Babich E. *J Vac Sci Technol B: Microelectron Nanometer Struct* 2002;20:2788.
- [201] Black CT, Guarini KW, Zhang Y, Kim H, Benedict J, Sikorski E, Babich IV, Milkove KR. *IEEE Electron Device Lett* 2004;25:622.
- [202] Ras RHA, Kemell M, De Wit J, Ritala M, Ten Brinke G, Leskelä M, Ikkala O. *Adv Mater* 2007;19:102.
- [203] Whitney AV, Elam JW, Zou SL, Zinovev AV, Stair PC, Schatz GC, Van Duyn RP. *J Phys Chem B* 2005;109:20522.
- [204] Wang XD, Graugnard E, King JS, Wang ZL, Summers CJ. *Nano Lett* 2004;4:2223.
- [205] Ruge A, Becker JS, Gordon RG, Tolbert SH. *Nano Lett* 2003;3:1293.
- [206] Ruge A, Park JS, Gordon RG, Tolbert SH. *J Phys Chem B* 2005;109:3764.
- [207] Scharer M, Wu X, Yamilov A, Cao H, Chang RPH. *Appl Phys Lett* 2005;86:15.
- [208] King JS, Heineman D, Graugnard E, Summers CJ. *Appl Surf Sci* 2005;244:511.
- [209] King JS, Graugnard E, Summers CJ. *Adv Mater* 2005;17:1010.
- [210] King JS, Graugnard E, Summers CJ. *Appl Phys Lett* 2006;88:8.
- [211] Graugnard E, Chawla V, Lorang D, Summers CJ. *Appl Phys Lett* 2006;89:21.
- [212] King JS, Graugnard E, Roche OM, Sharp DN, Scrimgeour J, Denning RG, Turberfield AJ, Summers CJ. *Adv Mater* 2006;18:1561.
- [213] Lee JH, Leung W, Ahn J, Lee T, Park IS, Constant K, Ho KM. *Appl Phys Lett* 2007;90:15.
- [214] Chen R, Kim H, McIntyre PC, Bent SF. *Appl Phys Lett* 2004;84:4017.
- [215] Chen R, Kim H, McIntyre PC, Bent SF. *Chem Mater* 2005;17:536.

- [214] Chen R, Bent SF. *Adv Mater* 2006;18:1086.
- [215] Chen R, Bent SF. *Chem Mater* 2006;18:3733.
- [216] Jiang XR, Chen R, Bent SF. *Surf Coat Technol* 2007;201:8799.
- [217] Jiang X, Bent SF. *J Electrochem Soc* 2007;154:D648.
- [218] Park KJ, Doub JM, Gougousi T, Parsons GN. *Appl Phys Lett* 2005;86:051903.
- [219] Hong J, Porter DW, Sreenivasan R, McIntyre PC, Bent SF. *Langmuir* 2007;23:1160.
- [220] Farm E, Kernell M, Ritala M, Leskel M. *Chem Vap Depos* 2006;12:415.
- [221] Bae C, Moon J, Shin H, Kim J, Sung MM. *J Am Chem Soc* 2007;129:14232.
- [222] Bae C, Shin H, Moon J, Sung MM. *Chem Mater* 2006;18:1085.
- [223] Sinha A, Hess DW, Henderson CL. *Electrochem Solid-State Lett* 2006;9:G330.
- [224] Sinha A, Hess DW, Henderson CL. *J Vac Sci Technol B: Microelectron Nanometer Struct* 2007;25:1721.
- [225] Sinha A, Hess DW, Henderson CL. *J Vac Sci Technol B: Microelectron Nanometer Struct* 2006;24:2523.
- [226] Lee BH, Ryu MK, Choi SY, Lee KH, Im S, Sung MM. *J Am Chem Soc* 2007;129:16034.
- [227] Lee KH, Choi J-M, Im S, Lee BH, Im KK, Sung MM, Lee S. *Appl Phys Lett* 2007;91:123502.
- [228] Cha SH, Oh MS, Lee KH, Im S, Lee BH, Sung MM. *Appl Phys Lett* 2008;92:023506.
- [229] Nanu M, Schoonman J, Gossens A. *Adv Mater* 2004;16:453.
- [230] Lu Y, Bangsaruntip S, Wang X, Zhang L, Nishi Y, Dai H. *J Am Chem Soc* 2006;128:3518.
- [231] Dalapati GK, Yi T, Wei-Yip L, Hoe Keat Mun AHKM, Byung Jin Cho ABJC. *IEEE Trans Electron Devices* 2007;54:1831.
- [232] Yang T, Xuan Y, Zemlyanov D, Shen T, Wu YQ, Woodall JM, Ye PD, Aguirre-Tostado FS, Milojevic M, McDonnell S, Wallace RM. *Appl Phys Lett* 2007;91:142122.
- [233] Xiang J, Lu W, Hu YJ, Wu Y, Yan H, Lieber CM. *Nature* 2006;441:489.
- [234] Keem K, Jeong DY, Kim S, Lee MS, Yeo IS, Chung UL, Moon JT. *Nano Lett* 2006;6:1454.
- [235] Choi BJ, Jeong DS, Kim SK, Rohde C, Choi S, Oh JH, Kim HJ, Hwang CS, Szot K, Waser R, Reichenberg B, Tiedke S. *J Appl Phys* 2005;98:033715.
- [236] Choi BJ, Choi S, Kim KM, Shin YC, Hwang CS, Cho Hwang S-Y, S-S Park S, Hong S-K. *Appl Phys Lett* 2006;89:012906.
- [237] Kim KM, Choi BJ, Koo BW, Choi S, Jeong DS, Hwang CS. *Electrochem Solid-State Lett* 2006;9:G343.
- [238] You Y-H, So B-S, Hwang J-H, Cho W, Lee SS, Chung T-M, Kim CG, An K-S. *Appl Phys Lett* 2006;89:222105.
- [239] Weatherspoon MR, Cai Y, Crne M, Srinivasarao M, Sandhage KH. *Angew Chem* 2008;120:8039.
- [240] Zhao Y, He S, Wei M, Evans DG, Duan X. *Chem Commun* 2010;46:3031.
- [241] Xiu Y, Hess DW, Wong CP. *J Colloid Interface Sci* 2008;326:465.
- [242] Yang J, Pi P, Wen X, Zheng D, Xu M, Cheng J, Yang Z. *Appl Surf Sci* 2009;255:3507.
- [243] Peng Y-T, Lo K-F, Juang Y-J. *Langmuir* 2010;26:5167.
- [244] Tiemann M. *Chem Eur J* 2007;13:8376.
- [245] Weatherspoon MR, Dickerson MB, Wang G, Cai Y, Shian S, Jones SC, Marder SR, Sandhage KH. *Angew Chem* 2007;119:5826.
- [246] Scott RWJ, Yang SM, Coombs N, Ozin GA, Williams DE. *Adv Funct Mater* 2003;13:225.
- [247] Song F, Su H, Han J, Xu J, Zhang D. *Sensors and Actuators B* 2010;145:39.
- [248] Guerra EM, Cestaroli DT, Oliveira HP. *J Sol-gel Sci Technol* 2010;54:93.
- [249] Jasty S. *Material Matters* 2006;1(2):3. <http://www.sigmaldrich.com/sigmaaldrich/technical-documents/articles/material-matters/introduction-to-molecular.html>.
- [250] Huie JC. *Smart Mater Struct* 2003;12:264.
- [251] DiBenedetto SA, Facchetti A, Ratner MA, Marks TJ. *Adv Mater* 2009;21:1407.
- [252] Palmer LC, Stupp SI. *Acc Chem Res* 2008;41:1674.
- [253] Przybyla DE, Chmielewski J. *Biochemistry* 2010;49:4411.
- [254] Kishimoto T, Morihara Y, Osanai M, Ogata S, Kamitakahara M, Ohtsuki C, Tanihara M. *Biopolymers* 2005;79:163.
- [255] Paramonov SE, Gauba V, Hartgerink JD. *Macromolecules* 2005;38:7555.
- [256] Cejas MA, Kinney WA, Chen C, Leo GC, Tounge BA, Vinter JG, Joshi PP, Maryanoff BE. *J Am Chem Soc* 2007;129:2202.
- [257] Kim DW, Ku B-C, Steeves D, Nagarajan R, Blumstein A, Kumar J, Gibson PW, Ratto JA, Samuelson LA. *J Membr Sci* 2006;275:12.
- [258] Dervishi E, Li Z, Watanabe F, Xu Y, Saini V, Biris AR, Biris AS. *J Mater Chem* 2009;19:3004.
- [259] Biris AR, Biris AS, Lupu D, Trigwell S, Dervishi E, Rahman Z, Marginean P. *Chem Phys Lett* 2006;429:204.
- [260] Dervishi E, Li Z, Biris AR, Lupu D, Trigwell S, Biris AS. *Chem Mater* 2007;19:179.
- [261] Biris AR, Lupu D, Gru'neis A, Ayala P, Ru'mmeli MH, Pichler T, Li Z, Xu Y, Misan I, Dervishi E, Biris AS. *Chem Mater* 2008;20:3466.
- [262] Dervishi E, Li Z, Watanabe F, Saini V, Biris AR, Xu Y, Biris AS. *Diamond Relat Mater* 2010;19:67.
- [263] Biris AR, Biris AS, Dervishi E, Li Z, Watanabe F, Simon S, Lupu D, Misan I, Lucaci M. *J Phys: Conference Series* 2009;182:012057.
- [264] Dervishi E, Li Z, Xu Y, Saini V, Biris AR, Lupu D, Biris AS. *Particulate Sci Technol* 2009;27:107.
- [265] Dervishi E, Li Z, Xu Y, Saini V, Watanabe F, Biris AR, Bonpain A, Garbay JJ, Meriet A, Richard M, Biris AS. *Particulate Sci Technol* 2009;27:222.
- [266] Meyyappan M. *J Phys D: Appl Phys* 2009;42:213001.
- [267] Kumar M, Ando Y. *J Nanosci Nanotechnol* 2010;10:3739.
- [268] See CH, Harris AT. *Ind Eng Chem Res* 2007;46:997.
- [269] Schedin F, Geim AK, Morozov SV, Hill EW, Blake P, Katsnelson MI, Novoselov KS. *Nat Mat* 2007;6:662.
- [270] Zhang Y, et al. *Appl Phys Lett* 2005;86:073104.
- [271] Fuhrer MS, Lau CN, MacDonald AH. *MRS Bulletin* 2010;35:289.
- [272] Booth TJ, et al. *Nano Lett* 2008;8:2442.
- [273] Avouris P, Chen Z, Perebeinos V. *Nat Nanotechnol* 2007;2:605.
- [274] Blake P, et al. *Nano Lett* 2008;8:1704.
- [275] Yoo E, Kim J, Hosono E, Zhou H, Kudo T, Honma I. *Nano Lett* 2008;8:2277.
- [276] Novoselov KS, et al. *Nature Phys* 2006;2:177.
- [277] Lemme MC, Echtermeyer TJ, Baus M, Kurz H. *IEEE Electr Device Lett* 2007;28:282.
- [278] Miao F, Wijeratne S, Zhang Y, Coskun UC, Bao W, Lau CN. *Science* 2007;317:1530.
- [279] Novoselov KS, et al. *Science* 2004;306:666.
- [280] Novoselov KS, et al. *Nature* 2005;438:197.
- [281] Novoselov KS, Jiang Z, Morozov SV, Stomer HL, Zeitler U, Maan JC, Boebinger GS, Kim P, Geim AK. *Science* 2007;315:1379.
- [282] Han MY, Ozyilmaz B, Zhang Y, Kim P. *Phys Rev Lett* 2007;98:206805.
- [283] Zhang Y, Tan YW, Stormer HL, Kim P. *Nature* 2005;438:201.
- [284] Tamura R, Tsukada M. *Phys Rev B* 1994;49:7697.
- [285] Wakabayashi K. *Phys Rev B* 2001;64:125428.
- [286] Zhang YB, Tan YW, Stormer HL, Kim P. *Nature* 2005;438:201.
- [287] Nakada K, et al. *Phys Rev B* 1996;54(17):954.
- [288] Morozov SV, Novoselov KS, Katsnelson MI, Schedin F, Ponomarenko LA, Jiang D, Geim AK. *Phys Rev Lett* 2006;97:016801.
- [289] Mayorov AS, Gorbachev RV, Morozov SV, Britnell L, Jalil R, Ponomarenko LA, Blake P, Novoselov KS, Watanabe K, Taniguchi T, Geim AK. *Nano Lett* 2011;11:2396.
- [290] Peres NM, et al. *Phys Rev B* 2006;73:125411.
- [291] Berger C, Song T, Li X, Li AY, Ogbazghi R, Feng Z, Dai AN, Marchenkov EH, Conrad PN First, Heer WADE. *J Phys Chem B* 2004;108:19912.
- [292] Faugeras C, Nerriere A, Potemski M, Mahmood A, Dujardin E, Berger C, Heer WADE. *Appl Phys Lett* 2008;92:011914.
- [293] Pisana S, Lazzeri M, Casiraghi C, Novoselov KS, Geim AK, Ferrari AC, Mauri F. *Nat Mater* 2007;6:198.
- [294] Novoselov KS, Jiang D, Schedin F, Booth TJ, Khotkevich VV, Morozov SV, Geim AK. *Proc Natl Acad Sci* 2005;102:10451.
- [295] Bruel M, et al. *Electron Lett* 1995;31:1201.
- [296] Ni ZH, Chen W, Fan XF, Kuo JL, Yu T, Wee ATS, Shen ZX. *Phys Rev B* 2008;77:115416.
- [297] Bommel AJV, Crombeen JE, Tooren AV. *Surf Sci* 1975;48:463.
- [298] Blake P, et al. *Appl Phys Lett* 2007;91:063124.
- [299] Zhang Y, Small JP, Amori MES, Kim P. *Phys Rev Lett* 2005;94:176803.
- [300] Echtermeyer TJ, Britnell L, Jasnok PK, Lombardo A, Gorbachev RV, Grigorenko AN, Geim AK, Ferrari AC, Novoselov KS. *Nat Comm* 2011;2:1.
- [301] Huc V, Bendiab N, Rosman N, Ebbesen T, Delacour C, Bouchiat V. *Nanotechnology* 2008;19:455601.
- [302] Stankovich S, Dikin DA, Dommett GHB, Kohlhaas KM, Zimney EJ, Stach EA, Piner RD, Nguyen ST, Ruoff RS. *Nature* 2006;442:282.
- [303] Obraztsov AN. *Nature Nanotechnology. News Views* 2009;4:212.
- [304] Kim KS, et al. *Nature* 2009;457:706.
- [305] Reina A, et al. *Nano Lett* 2009;9:30.
- [306] Cao H, et al. *J Appl Phys* 2010;107:044310.
- [307] Wang X, You H, Liu F, Li M, Wan L, Li S, Li Q, Xu Y, Tian R, Yu Z, Xiang D, Cheng J. *Chem Vap Deposition* 2009;15:53.
- [308] Dervishi E, Li Z, Watanabe F, Biswas A, Xu Y, Biris AR, Saini V, Biris AS. *Chem Commun* 2009;27:4061.
- [309] Dervishi E, Li Z, Watanabe F, Courte Au, Biswas A, Biris AR, Saini V, Xu Y, Biris AS. *Chem Mater* 2009;21:5491.
- [310] Dervishi E, Li Z, Shyaka J, Watanabe F, Biswas A, Umwungeri JL, Courte A, Biris AR, Kebdani O, Biris AS. *Chem Phys Lett* 2011;501:390.
- [311] Biris AS, Schmitt TC, Little RB, Li Z, Xu Y, Biris AR, Lupu D, Dervishi E, Trigwell S, Miller DW, Rahman Z. *J Phys Chem C Part of the special issue "Richard E Smalley Memorial Issue"* 2007;111:17970.
- [312] Nagata T, Ahmet P, Yamauchi Y, Sakuma Y, Sekiguchi T, Chikyow T. *Nucl Instr Meth B* 2006;242:250.
- [313] Wang Z, Liu X, Gong J, Huang H, Gu S, Yang S. *Crystal Growth & Design* 2008;8:3911.
- [314] Park WI, Lee CH, Chae JH, Lee DH, Yi GC. *Small* 2009;5:181.
- [315] Black K, Chalker PR, Jones AC, King PJ, Roberts JL, Heys PN. *Chem Vap Deposition* 2010;16:106.
- [316] Eilers H, Biswas A, Tyler TD, Norton MG, ElBahri M. *J Mater Res* 2006;21:2168.
- [317] Biswas A, Bayer IS, Marken B, Pounds TD, Norton MG. *Nanotechnology* 2007;18:305602.
- [318] Biswas A, Bayer IS, Tripathi A, Avasthi DK, Norton MG, Szczech JB. *Appl Phys Lett* 2007;91:212902.
- [319] Biswas A, Bayer IS, Karulkar PC, Tripathi A, Avasthi DK. *J Appl Phys* 2007;102:083543.
- [320] Bayer IS, Biswas A, Tripathi A, Avasthi DK, Singh JP, Magaridis CM. *Polymers for Advanced Technology* 2009;20:775.
- [321] Biswas A, Bayer IS, Dahanayaka DH, Bumm LA, Li Z, Watanabe F, Sharma R, Xu Y, Biris AS, Norton MG, Suhir E. *Nanotechnology* 2009;20:325705.
- [322] Biswas A, Bayer IS, Tripathi A, Lock EH, Walton SG, Norton MG, Avasthi DK, Bumm LA, Suhir E, Chowdhury AR, Gupta R. *Nanosci Nanotechnol Lett* 2009;1:111.
- [323] Biswas A, Marton Z, Kruse J, Kanzow J, Zaporotchenko V, Strunskus T, Faupel F. *Nano Lett* 2003;3:69.
- [324] Biswas A, Aktas OC, Schürmann U, Saeed U, Zaporotchenko V, Faupel F, Strunskus T. *Appl Phys Lett* 2004;84:2655.
- [325] Greve H, Pochstein C, Takele H, Zaporotchenko V, Gerber A, Frommberger M, Quandt E, Faupel F. *Appl Phys Lett* 2006;89:242501.

- [326] Takele H, Greve H, Pochstein C, Zaporojtchenko V, Faupel F. *Nanotechnology* 2006;17:3499.
- [327] Takele H, Jebril S, Strunskus T, Zaporojtchenko V, Adelung R, Faupel F. *Appl Phys A* 2008;92:345.
- [328] Faupel F, Zaporojtchenko V, Strunskus T, Elbahri M. *Adv Eng Mat* 2010;12:1177.
- [329] Beyene HT, Chakravadhanula VSK, Hanisch C, Elbahri M, Strunskus T, Zaporojtchenko V, Kienle L, Faupel F. *J Mater Sci* 2010;45:5865.
- [330] Greve H, Biswas A, Schürmann U, Zaporojtchenko V, Faupel F. *Appl Phys Lett* 2006;88:123103.
- [331] Elbahri M, Hedayati MK, Chakravadhanula VSK, Jamali M, Strunskus T, Zaporojtchenko V, Faupel F. *Adv Mater* 2011;23:1993.
- [332] Biederman H. *Vacuum* 2000;59:594.
- [333] Kuzuya A, Komiyama M. *Nanoscale* 2010;2:310.
- [334] Aldaye FA, Palmer AL, Sleiman HF. *Science* 2008;321:1795.
- [335] Chhabra R, Sharma J, Liu Y, Rinker S, Yan H. *Adv Drug Deliv Rev* 2010;62:617.
- [336] Lee JB, Campolongo MJ, Kahn JS, Roh YH, Hartman MR, Luo D. *Nanoscale* 2010;2:188.
- [337] Rothmund PWK. *Nature* 2006;440:297.
- [338] Andersen ES, Dong M, Nielsen MM, Jahn K, Subramani R, Mamdouh W, Golas MM, Sander B, Stark H, Oliveira CLP, Pedersen JS, Birkedal V, Besenbacher F, Gothelf KV, Kjems J. *Nature* 2009;459:73.
- [339] Han D, Pal S, Nangreave J, Deng Z, Liu Y, Yan H. *Science* 2011;332:342.
- [340] Kershner RJ, Bozano LD, Micheel CM, Hung AM, Fornof AR, Cha JN, Rettner CT, Bersani M, Frommer J, Rothmund PWK, Wallraff GM. *Nat Nanotechnol* 2009;4:557.
- [341] Hung M, Micheel CM, Bozano LD, Osterbur LW, Wallraff GM, Cha JN. *Nat Nanotechnol* 2010;5:121.
- [342] Ding B, Wu H, Xu W, Zhao Z, Liu Y, Yu H, Yan H. *Nano Lett* 2010;10:5065.
- [343] Pearson AC, Pound E, Woolley AT, Linford MR, Harb JN, Davis RC. *Nano Lett* 2011;11:1981.
- [344] Herr DJC. *J Mater Res* 2011;26:122.
- [345] Braun E, Eichen Y, Sivan U, Ben-Yoseph G. *Nature* 1998;391:775.
- [346] Keren K, Krueger M, Gilad R, Ben-Yoseph G, Sivan U, Braun E. *Science* 2002;297:72.
- [347] Keren K, Berman RS, Braun E. *Nano Lett* 2004;4:323.
- [348] Shukla S, Sastry M. *Nanoscale* 2009;1:122.
- [349] Le JD, Pinto Y, Seeman NC, Musier-Forsyth K, Taton TA, Kiehl RA. *Nano Lett* 2004;4:2343.
- [350] Liu J, Geng Y, Pound E, Gyawali S, Ashton JR, Hickey J, Woolley AT, Harb JN. *ACS Nano* 2011;5:2240.
- [351] Samano EC, Pilo-Pais M, Goldberg S, Vogen BN, Finkelstein G, LaBean TH. *Soft Matter* 2011;7:3240.